Development and Control
of a Modular and Reconfigurable Robot
with Harmonic Drive Transmission System

by

Zai Li

A thesis
presented to the University of Waterloo
in fulfillment of the
thesis requirement for the degree of
Master of Applied Science
in
Mechanical Engineering

Waterloo, Ontario, Canada, 2007

I hereby declare that I am the sole author of this thesis. This is the true copy of the thesis, including any required final revisions, as accepted by examiners.

I understand that my thesis may be made electronically available to the public.

Zai Li

Abstract

This thesis presents a detailed design, calibration, and control of a modular and reconfigurable robot (MRR) system. A MRR system not only includes modular mechanical hardware, but also modular electrical hardware, control algorithms and software. Also, those modular components can be easily constructed into various manipulator configurations to accomplish a wider range of tasks. MRRs represent the next generation of industrial manipulators that cope with the transition from mass to customer-oriented production.

The main contributions of this thesis are: 1) mechanical design and calibration of multi-input multi-output (MIMO) joint modules of MRR, and 2) control design to handle multiple configuration and overcome disturbance due to dynamics uncertainty. From the mechanical design point of view, this thesis presents two main topics: 1) each joint is not only modularly designed, but also has multiple-input multiple-output (MIMO) physical connection ports, which contributes to the concept of reconfigurability. Strictly speaking, single-input single-output (SISO) modular joint falls into the category of modular manipulator, and the robot reconfiguration is achieved by integrating different types of modules. For example, with single revolute MIMO joint module, both rotary and pivotal joint can be generated. On the other hand, if you would like to switch from rotary movement to pivotal movement with a SISO joint module, using another pivotal joint module is the only way to achieve this goal, and 2) for precise automation application, joints and links should be accurately connected and oriented when reconfigured.

Our proposed modular joint has four connection ports which can be configured as either a rotary joint or a pivotal joint. In addition, key and keyway connection mechanism provides high accuracy in positioning the link onto the joint. Therefore, this structure reduces or eliminates MRRs system calibration time when reconfigured. Furthermore, zero link offset when used as a pivotal joint increases the robot dexterity, maximizes the reachability, and results in kinematics simplicity.

The main challenge in the control of an MRR system with harmonic drives (HD) is the significant uncertainties due to friction, unmodelled dynamics, varying payload, gravitation, dynamic coupling between motions of joints, and the configuration changes. In order to compensate all unpredictable effects, we proposed a decentralized saturation-type robust control scheme based on direct-Lyapunov method and backstepping techniques. To

better understand the system dynamics behavior, the HD flexspline compliance and friction calibration and results are also provided. The results are used for controller design. The proposed controller is verified through both computer simulation and experimental analysis.

Acknowledgements

I would like to take this opportunity to thank my supervisor, Dr. William W. Melek and Dr. Christopher M. Clark, for their guidance, encouragement, and support throughout this project.

I would also like to thank Dr. Jan Paul Huissoon and Dr. John Yeow for agreeing to read my thesis.

I would like to thank Mr. Saleh Tabandeh, Mr. Mohsen Shahini and other group members for their assistant.

Finally, I would like to thank my family for their understanding, encouragement and supporting.

Contents

List of Tables

List of Figures

xi

Glossary

$D(q_1)$ n×n symmetric, positive definite inertial matrix

$C(q_1, \dot{q}_1)$ matrix containing coriolis, centripetal, friction and gravitational forces and torques

J_{mw} motor rotor and HD wave-generator inertial

F_{md}, F_{ms} motor viscous and Coulomb friction coefficients

K_{s1},K_{s2} flexspline stiffness coefficients

q_2,$\dot{q}_2$,$\ddot{q}_2$ motor position, velocity and acceleration

N HD gear reduction ratio

τ motor input torque

J_l link and load inertia

m link mass

l link length

F_{ld},F_{ls} harmonic drive viscous and Coulomb friction coefficients

q_1,$\dot{q}_1$,$\ddot{q}_1$ link position, velocity and acceleration

τ_d disturbance torque

Chapter 1

Introduction

1.1 Motivation

This research project was initiated to tackle a need by an industrial partner, Sterner Automation, for a flexible automation setup to handle a variety of automotive assembly tasks. One of the immediate tasks that require automation involves assembly of four screws on a car back-seat as shown in Fig. (1.1). This task is currently done by skilled workers in plants at Ford and General Motive (GM). But in a fast-paced manufacturing environment, it is hard for workers to keep up with the high operation speed of the manufacturing line and the variety of tasks. In fact, a solution is available: an existing industrial manipulator can be programmed to perform this task with accuracy and reliability. But considering the company's needs for a flexible automation system, a modular and reconfigurable robot (MRR) system is the better choice. Because the MRR system can be reconfigured to cope with more complex tasks that can not be accomplished using fixed-configuration manipulators, the company will benefit from the MRR in automating several tasks such as auto seat assembly, cushion fastening, and seat rotation, etc.

To address this need, we developed a 3-DOF MRR system that can be integrated with an endpoint wrist and an end tool to perform various industrial tasks. The following requirements were created as the framework of the system development:

- 3-DOF robot system coupling with an end tool is needed to complete the seat as-
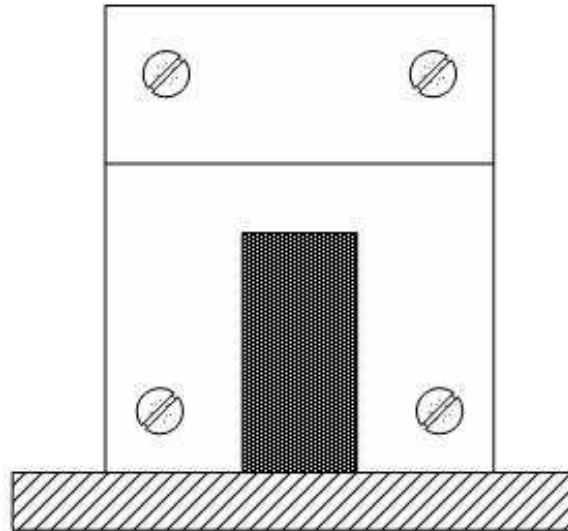
Figure 1.1: Car back-seat installation

sembly task .

- Joint modules should have multiple input multiple output mechanical ports to increase mechanical flexibility.

- Joint velocity is in the range of 20-40rpm to meet the assembly line throughput requirement.

- The output power is in the range of 300-1000w for a wide range of applications.

- Size and weight should be as small as possible, which depend on the selected hardware.

The objective of this project is to develop and control such a MRR system that matches the above specifications. Before the introduction to detailed mechanical design and control algorithm development, we first review backgrounds of the existing MRR structures, HD modeling that is used in the MRR single joint dynamic model, and the control theory.

1.2 Modular and Reconfigurable Manipulators

Defined by the Robot Institute of America (RIA), a robot refers to a reprogrammable and multifunctional manipulator designed to move material, parts, tools, or specialized devices through variable programmed motions for the performance of a variety of tasks. The reprogrammability points out the robot's adaptability. Since George Devol designed the first programmable robot in 1954, robot manipulators have been widely used, especially in the automobile industry. Given the success in the automobile industry, other industries, eg. nuclear, space, electronics manufacturing etc., started to apply robots to some dangerous, dirty, difficult or repeated tasks. Reprogrammable robots exhibit tremendous advantages in mass production environments. But with the fast growth of economy, customer-oriented production is becoming more dominant in today's markets. In this case, the application of reprogrammable robots is limited by its mechanical constraints. To respond to rapid changes of product design, manufacturers need a more flexible fabrication system. In recent years, modular and reconfigurable robots (MRRs) were proposed to fulfill the requirements for the flexible production system.

MRRs refer to three types of robots: 1) modular and reconfigurable serial robot [1]-[4], 2) modular and reconfigurable parallel robot [5]-[8], and 3) modular self-reconfigurable robot [9]-[14]. The first type of MRR is the focus of this research. This type of robot can be used in manufacturing industry, for example, welding, pick-and-place, assembly, material cutting, etc. Similar to serial robots, modular and reconfigurable parallel robots consist of a collection of individual standard units that can be assembled into various parallel robot configurations. Modular and reconfigurable parallel robots can be used as a platform for flexible automation. For example, in [8], a modular and reconfigurable parallel robot manipulator was developed and prototyped. Fig. (1.2) shows such a robot holding a tool to grind a workpiece. A theoretical design reconfigurable machine tools using modular design approach is presented in [7] (Fig. (1.3)).

Unlike the first two types of MRR which are reconfigured by humans, modular self-reconfigurable robots refer to structures that have the ability to change their configuration by themselves. The snake-shape modular self-reconfigurable robot is one of this type, and it consists of a large number of modular cells. One commonly used mechanical cell structure is shown in Fig.(1.4), and the robot built from it is shown in Fig.(1.5). In [14],

Figure 1.2: Parallel robot for machining [8]
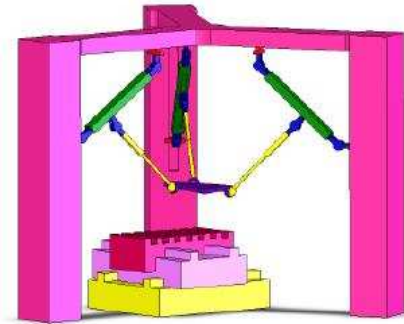
Figure 1.3: 5-axis parallel kinematic machine [7]

the authors proposed a mobile type of self-reconfigurable robot as shown in Fig. (1.6). It is constructed with mobile vehicles with a passive joint between them. A quick-connect mechanism utilizing rare-earth magnets is used to attach modules, and a release mechanism allowing bodies to intentionally disconnect and provide automatic separation in the event of power failure of a particular body. Another type of self-reconfigurable parallel robot is proposed in [6]. This type of robot is able to self-reconfigure to other types of planar parallel robot on a horizontal plane as shown in Fig. (1.7). An application example is also given in [6].

Figure 1.4: Module cell for snake-shape self-reconfigurable robots [12]
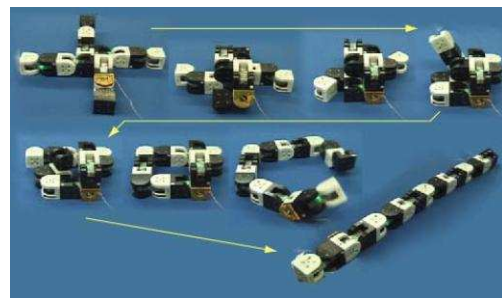
Figure 1.5: Snake-shape self-reconfigurable robot [12]

In this thesis, we developed a novel MRR with a harmonic drive (HD) transmission sys-

Figure 1.6: Mobile type self-reconfigurable robot [14]
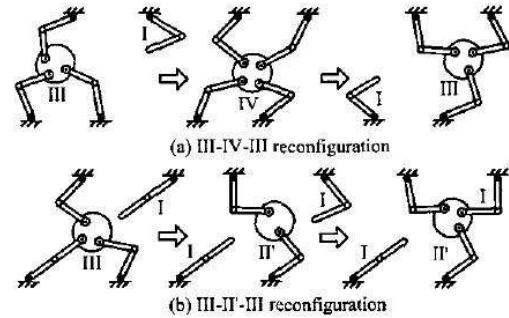
Figure 1.7: Self-reconfigurable parallel robot [6]

tem for automation of industrial tasks such as car seat assembly. The MRR in this thesis refers to the modular and reconfigurable serial robot. As mentioned above, reconfigurability is a major advantage of MRR, but with changing configurations, the robot dynamic parameters also change. Therefore, controllers designed based on one configuration may not work well when the MRR is reconfigured. This is why a decentralized control technique is applied in our research. In decentralized control, each joint is considered as an independent subsystem, and the dynamic effects from the other links and joints are treated as disturbance [18]. Furthermore, more uncertainties exist due to the unmodeled dynamics, HD flexspline compliance, HD complex gear meshing mechanisms and varying payloads. A robust control law has the ability to compensate for external disturbances. Therefore, a decentralized robust controller was developed, and the detailed stability analysis and experimentation are also provided in this thesis.

1.3 Literature Review

As an application of the concept of a modular system, a MRR system refers to an entire manipulator that includes not only the modular mechanical hardware, but also modular electrical hardware, control algorithms and software [2]. In [15], a MRR system is defined as a collection of individual link and joint components that can be easily assembled into a variety of configurations and different geometries. The author in [16] states that the MRR

system would replace most current fixed configuration industrial robots in the future.

Much work has been done to develop MRR systems. In summary, these works include hardware design and integration, control software development, and configuration optimization for specific task. Hardware design refers to both mechanical and electrical components structure design, link/joint connection mechanism, and system integration. Dedicated software is used for the MRRs precision motion control, for which the system dynamics should be fully understood. Configuration optimization is an algorithm which provides the best MRR configuration for a given task based on some criteria, i.e. minimal number of degree of freedom needed, minimal power consumption, maximum speed and reachability, etc. Configuration optimization is out of the scope of this thesis.

1.3.1   MRR Structure Development

Modularity and reconfigurability are two basic requirements of the MRR system. The concept of modularity has been deployed in many engineering disciplines for a long time. It refers to dividing a complicated system into different modules with high portability, ease of maintenance. Modularizing system components can also decrease the design and manufacturing time. From the mechanical structure perspective, a robot system is a collection of joints and links which are connected with each other to build a configuration that can perform a variety of tasks. Using modular joints and links, different configurations can be constructed, which is the concept of the reconfigurable robot. But strictly speaking, only a modular joint module with multiple-input multiple-output (MIMO) connection ports is able to reconstruct different configurations by reconfiguring itself. How many configurations can be generated with a specific number of modular joints and links depends on the joints type, i.e. rotary/prismatic, the number of degree of freedom, and the number of physical connection ports on the modular joint.

Several prototype modular robotic systems have been built and demonstrated. The reconfigurable modular manipulator system (RMMS) in [2] consists of two types of 1-DOF revolute joints: rotate and pivot joint, which are actuated by DC motors in conjunction with harmonic drive mechanisms, and links of circular cross-section. Commercial V-band clamps are used for joints and links integration. Each joint houses the power and sensor electronics for the actuator. A Local Area Network (LAN) like link is used for communica-

tion between joints and controller. A task based design method is introduced in [17]. The developed manipulator is composed of three modules: base unit, link module and two pivot joint modules. In addition, a quick-coupling mechanism is deployed, with which a secure mechanical connection between modules can be achieved by simply plugging by a hand with no tools required. The most important contribution of the paper is that the authors introduce an efficient Genetic Algorithm (GA) to determine the necessary configuration of the modular robot manipulator with minimal number of degrees of freedom to perform a given task trajectory. The authors in [19] proposed a rapidly deployable manipulator system. Compared with most industrial manipulators that have a separate unit housing the sensor interface, power amplifiers, control processors and other electronics, the proposed system has self-contained hardware modules. In other words, the single module contains all control hardware, i.e. sensors, an actuator, a brake, a transmission, a sensor interface, a motor amplifier, and a communication interface. The most important advantage of this design is that it reduces wiring for power distribution and data communication. In addition, integrated quick-coupling connectors provide quick connection between modules. The modular and reconfigurable control software is developed using the Chimera real-time operating system [20]. This software has the ability to automatically build kinematic and dynamic models of the entire manipulator based on a data file created during initialization phase. Researchers in the Robotics Research Center of Nanyang Technological University have built a rapidly reconfigurable robotic workcell [21], which includes standard and inter-operable components. A prototype of the robotic workcell has been demonstrated in the International Industrial Automation Exhibition in Singapore. This workcell consists of a 7-DOF redundant serial robot to pick and place the workpiece, one 6-DOF parallel modular robot to machine the workpiece, and a 1-DOF linear motion stage to move the workpiece in between the two robots, as shown in Figure 1.8. The other MRR system can be found in [22][23][24].

From the mechanical structure point of view, the joint module is the core component of the MRR system. Six types of joints are commonly used: revolute joint (1-DOF), prismatic joint (1-DOF), screw joint (1-DOF), cylindrical joint (2-DOF), planar joint (2-DOF), and spherical joint (3-DOF) [25]. Based on the motivation described above, a PUMA type configuration is able to accomplish the task of car back-seat installation; therefore, only the

Figure 1.8: Reconfigurable robotic workcell (Nanyang Technological University)[21]

revolute joints are considered in our research, which includes rotational and pivotal joints. A rotational type joint has a link length which is co-linear with the joint axis. A pivotal one has a link length which is perpendicular to the joint axis. By carefully examining the revolute joint modules developed by researchers as shown in Fig. (1.9), their common features can be summarized as: 1) one-degree of freedom of motion; 2) use the harmonic drive to transmit power; 3) single input single output (SISO) physical connection port, except for the cubic shape joint module, which has multiple connection ports. Therefore, the cubic shape module can be used as either a rotary joint or a pivotal joint, but the link offset "d" is generated when used as a pivotal joint as shown in Fig. (1.10). The other SISO modules have to be used together in order to generate a new robot configuration.

In this research, we have developed a joint module which has four physical connection ports so that a variety of manipulator configurations can be constructed using the single type of module. The detailed design and calibration procedures of the development joint module can be found in chapter 2.
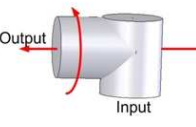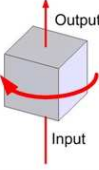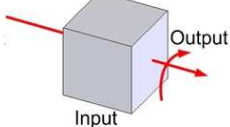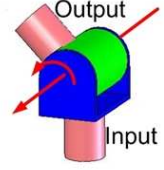
Figure 1.9: Commonly used MRR joint modules
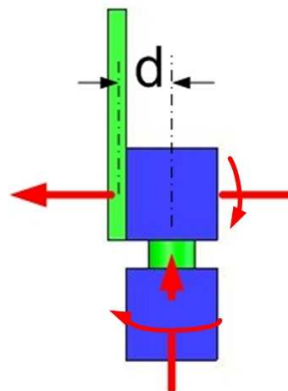
Figure 1.10: 2DOF module with cubic joints ("d" is the link offset)

1.3.2   Harmonic Drive Modeling

Compact size and high power transmission capability are the two most important reasons why the harmonic drive (HD) is widely used by robot designers. Zero backlash is definitely one of the advantages of the HD, but the thin wall of the flexspline generates deformation when torque is applied, due to elasticity. Therefore, the stiffness of the flexspline largely affects the accuracy in motion control. The HD exhibits more complex dynamic behavior than conventional gear transmission system. Usually, simple models are used for MRR with HD transmission system controller design [26]. The commonly used model is the combination of linear compliance, viscous friction and Coulomb friction. But HD dynamic behavior is quite nonlinear. One of contributions of this research is that we set up experiments to characterize the nonlinearities of HD dynamics, so that a more accurate robot model is used to design the controller. In this subsection, the literature review of HD modeling methods are presented, and our calibration setup and results are introduced in chapter 3.

Developed in 1955, the HD was primarily introduced for aerospace applications. It has three components as shown in Fig. (1.11): wave generator, flexspline and circular spline. The nonlinear dynamic behavior comes from the non-rigid flexspline. HD mathematical models based on experiments were developed in [27]. In this paper, the authors modeled a HD system component by component. The motor-amplifier subsystem is modeled as a "torque source" with a limiting capability, due to the action of the back emf and the current limiter of the amplifier. This "torque source" applies a torque to the input inertia, which includes the motor armature and the HD wave generator. This subsystem is considered as a mass-friction system with saturated torque. Three physical phenomena related to the flexspline subsystem are: nonlinear stiffness, hysteresis, and quasi-backlash due to soft-windup effect. A cubic polynomial is used for nonlinear stiffness model, and the soft-windup correction factor is modeled as a saddle-shaped function. The hysteresis curve is matched by friction. The circular spline is also modeled as a mass-friction system. A more detailed model can be found in [28]. In this paper, three models are developed: 1) a friction model which consists of velocity-independent friction, velocity-dependent friction and friction from resonant vibration; 2) compliance model which is a cubic function; 3) kinematic error is modeled as sum of sinusoidal functions. Other HD models can also

be found in [29][30]. In this research, the HD system is modeled as a nonlinear cubic function together with a velocity-dependent and velocity-independent friction model which is described in the design section.
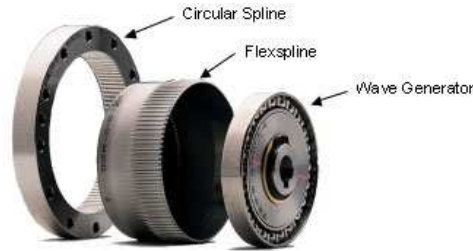
Figure 1.11: Harmonic drive components

1.3.3   Robot Manipulator Control Theory

The selection of the control law not only depends on the robot mechanical design, i.e. rotary joint robot and Cartesian manipulator, but also relies on the model used. Based on the assumption made on the manipulator's joints, links, and the control signal, six manipulator models are commonly encountered in the literature: 1) torque level rigid link rigid joint (TLRLRJ) [31][32][33]; 2) electrically driven rigid link rigid joint (EDRLRJ)[34]; 3) torque level rigid link flexible joint (TLRLFJ) [26][35][40]; 4) electrically driven rigid link flexible joint (EDRLFJ)[37]; 5) flexible manipulator (FM) [38]. A considerable number of control techniques and methodologies have been created and applied to the control of manipulators in the past. In this research, the controller development is based on TLRLFJ.

Joint flexibility is a major source of oscillatory behavior of the manipulator, and considerably affects robot's performance. A widely acceptable TLRLFJ model was introduced in [39], where the robot is being modeled as two second order differential equations under the assumption: 1) the joints are purely rotary; and 2) the rotor/gear inertia is symmetric about the rotation axis. This dynamic model is shown to be globally linearizable and a nonlinear control is provided based on a singular perturbation formulation of the equations of motion and the concept of integral manifold, but the author did not prove the stability

of the system. Based on the same theories, a composite control algorithm with detailed stability analysis is proposed in [40], which consists of a fast control and a slow control. In [41], a fuzzy supervisor is added to decrease the fast controller bandwidth at critical occasions, i.e. near saturation point which could cause instability.

Robust control is the most commonly used methodology for complex systems, especially for the manipulator control. [42] presents a summary of robust control method before 1997 in the categories of linear, passivity-based, Lyapunov-based, sliding mode, nonlinear and robust adaptive control schemes. [43] provides detailed design procedure of centralized Lyapunov-based robust control for an n-dof manipulator under joint flexibility. [44] standardizes some robust controller, such as saturation type controller, passivity controller, etc. For decoupled joint controller, each joint is considered as a single input single output (SISO) subsystem. A general form of decentralized sliding mode robust control law is proposed in [45] for any mechanical system described by Euler-Lagrange equation and involving high-order interconnections. In [46], another simple decentralized nonlinear control algorithm is developed. This controller has three integral terms in the tracking error, and a systematic method for controller parameters selection is also provided. But those controllers [45][46] are designed for TLRLRJ. In [47] linear PD/PID compensator have been designed in the presence of actuator saturation and transmission flexibility. Other controllers, such as PD/PID with gravitational compensation, intelligent fuzzy controller, etc., can be found in [48][49][50][51][52]. In this thesis, a decentralized robust controller for MRRs with HD has been proposed using Lyapunov-based method and backstepping techniques.

1.4 Contributions

This thesis provides contributions in two different areas of modular and reconfigurable robot (MRR) development: 1) mechanical design, and 2) control software. In specific terms, the contributions of this reseach are:

Mechanical Design and Manufacturing of a MRR:

- We designed modular manipulator joints in three different size and output power

ranges. Each joint module has four physical connection ports so that it can be constructed as either a rotary joint or a pivotal joint. Together with cylinder type rigid link, different robot configurations can be generated to perform a wide variety of tasks. In addition, zero link offset in pivotal joint increases the robot dexterity, maximizes the reachability, and results in kinematics simplicity. Furthermore, key and keyway coupling between joints and links provides high accuracy in position and orientation when reconfigured. Chapter 2 describes this mechanism in detail.

MRR Control Software Development:

- Due to the elasticity of the harmonic drive (HD) flexspline, the proposed modular and reconfigurable robot (MRR) system exhibits dynamic disturbance that has to be addressed. We developed a decentralized saturation-type robust control scheme based on Lyapunov's stability analysis and backstepping techniques to compensate all unpredictable disturbance. The proposed controller was tested through both computer simulation and experiments.

1.5   Thesis Organization

The organization of this thesis is as followed:

Chapter 2 describes the detailed modular and reconfigurable robot (MRR) system design. This includes design of joint module, link module and MRRs integration.

Chapter 3 introduces the MRR dynamics. Because developing a decentralized controller is an objective, we only focused on the single joint dynamics, and the effect of the successive link/joint is considered as disturbance. In addition, a nonlinear HD compliance model was used to capture higher-order MRR dynamics.

Chapter 4 provides the decentralized robust controller development. The controller was created based on direct-Lyapunov method and backstepping techniques. The detailed stability analysis is presented.

In chapter 5, the controller validation results are presented. Both computer simulation and experimental method are used to validate the proposed control algorithm.

The conclusion and future work are presented in chapter 6.

Chapter 2

MRR Mechanical Design

2.1 Introduction

Selecting suitable and economical hardware components is one of factors that determines if the design is optimal or not. There is a wide variety of on-the-shelf hardware components available for our project. For example, we can use direct drive torque motor which can deliver high torque at low velocity, but is too expensive. The smart motor integrates servo, drive and controller into a single unit. Coupled with a transmission system, smart motor may be the best choice for MRR system integration from the point view of modularity, but results in a larger and heavier joint module. As a practical and effective alternative, we use conventional brushless DC motor (Fig.(2.1)) with a harmonic drive (HD) (Fig. (1.11)) transmission system, and a separate drive controller unit placed away from the physical joint. Two thin section bearings from KAYDON BEARINGS (Fig.(2.2)) are used to support HD. All hardware components and their specifications are listed in tables (2.1),(2.2),(2.3) and (2.4). Those hardware components were selected based on the power, velocity and output torque requirements of each joint module.

Figure 2.1: AKM series motor and drive

Figure 2.2: Thin section bearing

Table 2.1: MRR hardware: Motor (Fig. (2.1))

	Rated Torque (Nm)	0.81
Smallest Joint (AKMS20360)	Rated Speed (rpm)	3500
	Rated Power (W)	300
	Rated Torque (Nm)	1.96
Medium Joint (AKMS20360)	Rated Speed (rpm)	3000
	Rated Power (W)	620
	Rated Torque (Nm)	4.08
Largest Joint (AKMS20360)	Rated Speed (rpm)	2500
	Rated Power (W)	1070

Table 2.2: MRR hardware: Driver (Fig. (2.1))

Smallest Joint	Power Input (VAC)	120/240
	Control Mode	torque, velocity and position
	Feedback Signal	torque, velocity and position
Medium Joint	Power Input (VAC)	120/240
	Control Mode	torque, velocity and position
	Feedback Signal	torque, velocity and position
Largest Joint	Power Input (VAC)	120/240
	Control Mode	torque, velocity and position
	Feedback Signal	torque, velocity and position

Table 2.3: MRR hardware: Harmonic Drive (Fig. (1.11))

Smallest Joint (CSF-32)	Reduction Ratio	100
	Max Input Speed (rpm)	4800
	Rated Torque (Nm)	137
	Moment of Inertia ($\times 10^{-4} kgm^2$)	1.72
Medium Joint (CSF-40)	Reduction Ratio	100
	Max Input Speed (rpm)	4000
	Rated Torque (Nm)	265
	Moment of Inertia ($\times 10^{-4} kgm^2$)	4.59
Largest Joint (CSF-50)	Reduction Ratio	100
	Max Input Speed (rpm)	3500
	Rated Torque (Nm)	696
	Moment of Inertia ($\times 10^{-4} kgm^2$)	27.9

Table 2.4: MRR hardware: Bearing (Fig. (2.2))

Smallest Joint (K10008CP0)	Bore Dia. (mm)	100
	Outside Dia. (mm)	116
	Static Radial Load (kg)	1061
	Dynamic Radial (kg)	507
	Weight (kg)	0.14
Medium Joint (K14008CP0)	Bore Dia. (mm)	140
	Outside Dia. (mm)	156
	Static Radial Load (kg)	1465
	Dynamic Radial (kg)	613
	Weight (kg)	0.18
Largest Joint (K17008CP0)	Bore Dia. (mm)	170
	Outside Dia. (mm)	186
	Static Radial Load (kg)	1767
	Dynamic Radial (kg)	686
	Weight (kg)	0.2

2.2   Joint Design

Simply speaking, joint module design is the processing of integrating motor and gear transmission system with the help of bearing and coupling. We proposed a novel joint module architecture that has two mechanical inputs and two outputs as shown in Fig. (2.3). Fig. (2.4) and (2.5) show the joint module with link(s).The specifications are listed in Table (2.5).The key features are summarized as followed: 1) each module has four physical connection ports; 2) parts 1, 2, 3 can be disassembled depending on the configuration to reduce the weight, i.e. rotary or pivotal joint,; 3) links can be precisely positioned onto the joint by four keys/keywarys separated 90 deg with respect to each other. This structure not only minimizes the positioning error, but also provides accurate 90 deg link twist angle; 4) the zero link offset in pivotal rotation increases the robot dexterity, maximizes the reachability, and results in kinematics simplicity.
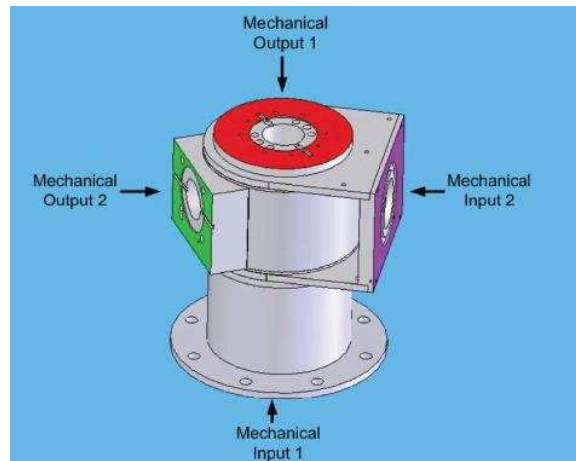
Figure 2.3: Proposed joint module

2.3   Link Design

In contrast to joint module, link module is easier to design. Except for the mechanical structure requirements, i.e. the connectivity to the joint module, the rigidity is the only
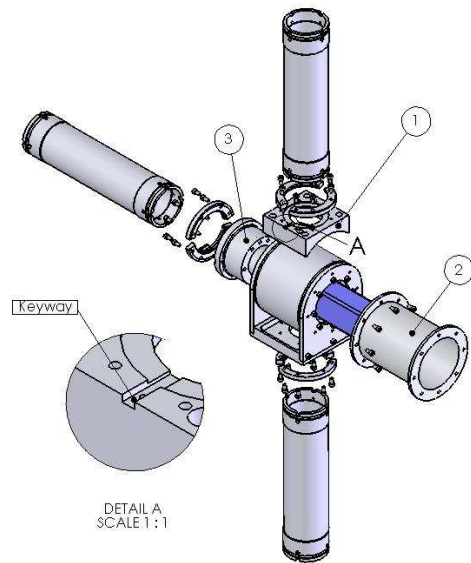
Figure 2.4: Proposed joint module with Links

Figure 2.5: MRR rotary joint built at UW

Table 2.5: MRR specifications

	Smallest		Medium		Largest	
	Pivotal	Rotational	Pivotal	Rotational	Pivotal	Rotational
Power (W)	300	300	700	700	1000	1000
Velocity (rpm)	35	35	30	30	25	25
Torque (Nm)	81	81	196	196	408	408
Weight (kg)	12.5	10.5	18	16	25	23
Size (mm)	$\phi 120 * 210$		$\phi 170 * 300$		$\phi 200 * 400$	
Range (deg)	130	360	130	360	130	360
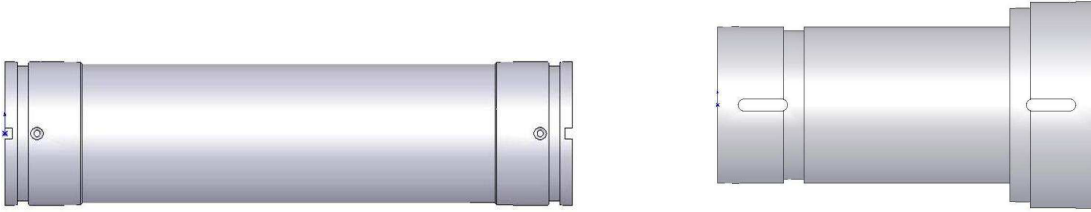
Figure 2.6: Two types of Link modules

requirement. In order to connect the proposed joint modules, two types of link tubes with different diameters were designed as shown in Fig. (2.6). The length of those links was selected to ensure reachability for the industrial task described in Fig. (1.1).

2.4 MRR Configurations

Using the designed link and joint modules, different MRR configurations can be constructed. Robot kinematic configuration refers to the mechanical arrangement of the joints and links in a robot. It is defined by the number of DOF, dimension of the links, and the orientation between two consecutive joint axes. The total number of configurations can be generated depends on the number of degree of freedom of each joint, number of connection ports, number of modules being used and types of links. In our case, each joint has four ports and three modules are used. We consider only one type of link, because the link we

designed is used to connect two joints with different connection dimensions. Therefore, the total number of configurations are calculated based on the following equation

$$
\begin{aligned}
x &= a^b \\
&= 4^3 \\
&= 64
\end{aligned}
\tag{2.1}
$$

Where x is the number of configurations; a is the number of connection ports; and b is the number of modules.

Not all configurations are useful because of the singularity. The robot configuration can be described using standard Denavit-Hartenberg (DH) notation with four parameters: link length a_i, link offset d_i, twist angle α_i and joint angle θ_i. The most commonly encountered configuration is the PUMA configuration shown in Fig. (2.7), and its standard DH table is shown in Fig. (2.8). Noticed that the offset of $l_b - l_d$ in link 3 of the original PUMA is eliminated in our design as shown in Fig.(2.9). The PUMA robots are mainly used for small part assembly, and robots with PUMA configuration have an extensive industrial applications, e.g. welding, material handling, cutting, medical surgery, etc.
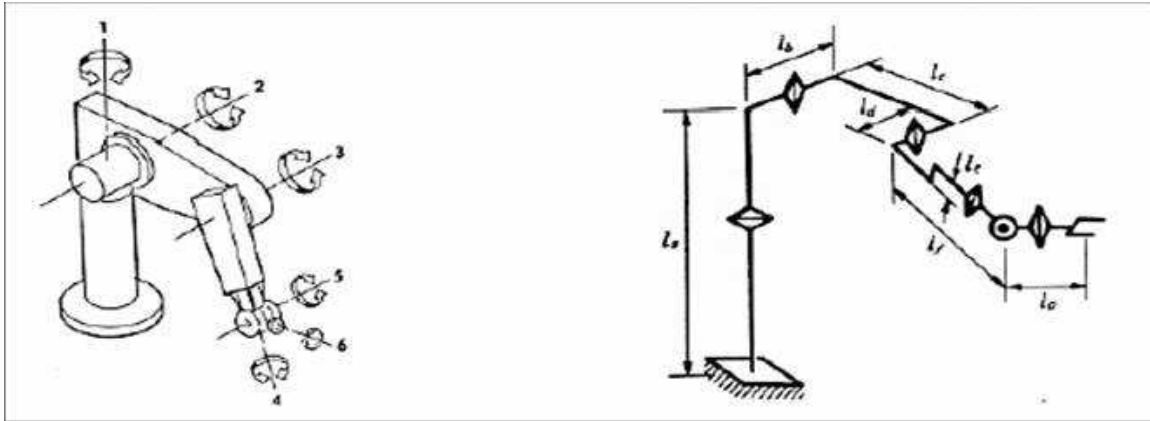
Figure 2.7: PUMA 560 robot and schematics

Another robot configuration is Selective Compliant Assembly Robot Arm (SCARA) robot, which is shown in Fig.(2.10) and (2.11).In general, the SCARA robots can move to

i	a_i	α_i	d_i	θ_i
1	0	$-90°$	0	θ_1 $(0°)$
2	l_c	$0°$	$(l_b - l_d)$	θ_2 $(0°)$
3	l_e	$-90°$	0	θ_3 $(0°)$
4	0	$90°$	l_f	θ_4 $(0°)$
5	0	$-90°$	0	θ_5 $(0°)$
6	0	$0°$	0	θ_6 $(0°)$

Standard Denavit Hartenberg
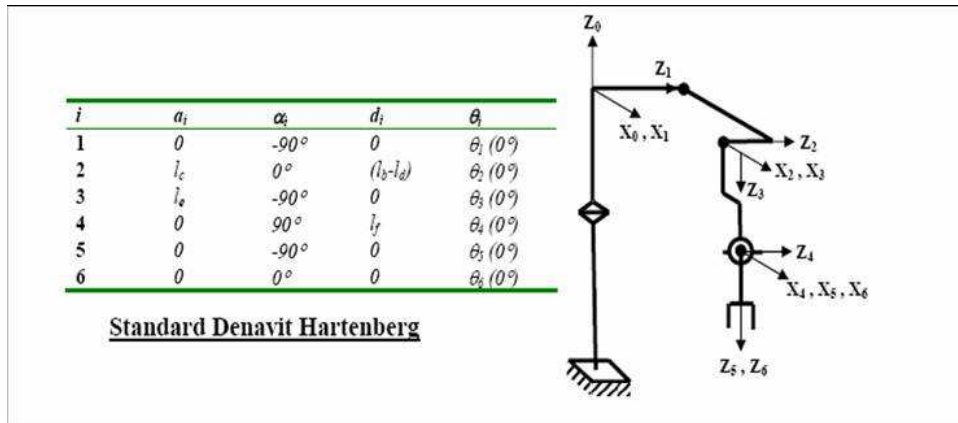
Figure 2.8: PUMA standard DH
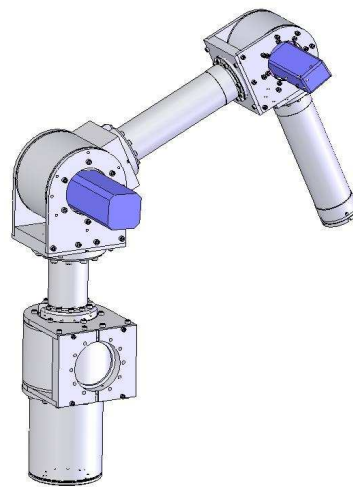
Figure 2.9: Proposed MRR in PUMA configuration

any X-Y coordinate within their work envelope, and vertical motion in Z direction can be achieved by integrating an independent linear axis at the wrist or in the base. SCARA robots are widely used in pick-and-place, assembly, and packaging applications. In micro-electronics industry, they are used to place semiconductor ICs and other components on the computers circuit boards.
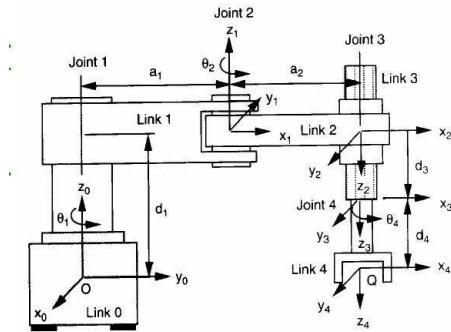
Figure 2.10: SCARA robot
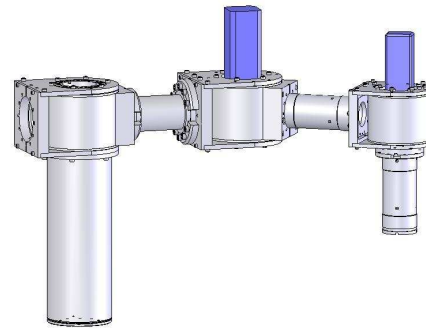
Figure 2.11: Proposed MRR in SCARA configuration

With the designed joint and link modules, many other type of configurations can also be generated. Fig.(2.12) shows an example of some of such configurations.

2.5   Discussion

In summary, the designed joint module and link module are introduced in this chapter. Two input and two output ports structure enable more configurations to be generated. Due to the time and budget issues, there exist three minor unresolved issues even though the proposed design has satisfied the original functionality objective. First, the joint module is larger and heavier than expected. If frameless motor is used instead of housed motor, the size and weight of each joint will be reduced, but will increase the design and integration complexity. Second, in order to reduce the manufacturing cost, some parts which can be welded together are connected using screws, which increases the MRR's installation time
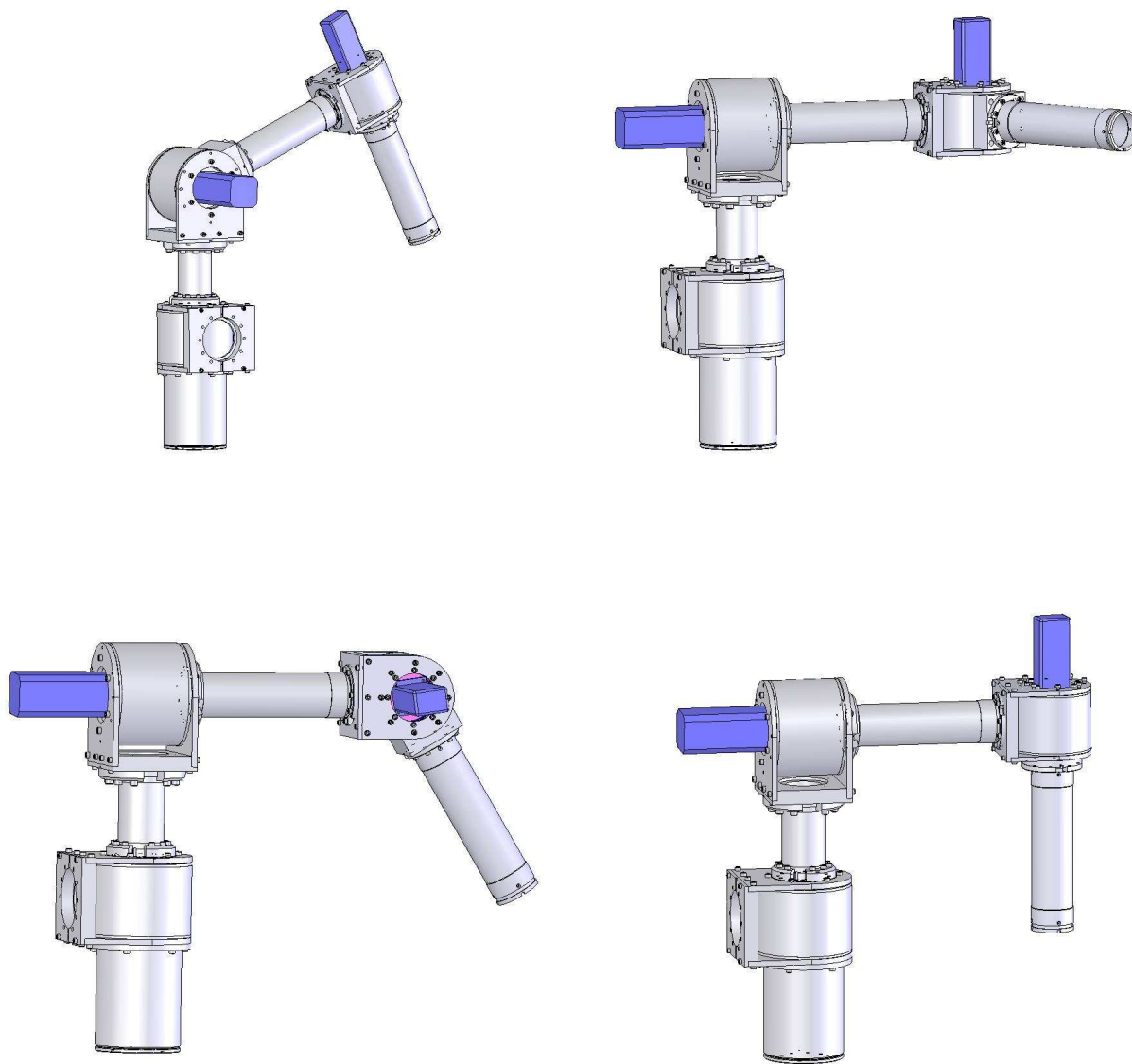
Figure 2.12: Other types of MRR configurations

when reconfigured. Third, how to run all cables and wires internally is still a challenging task for us. To solve this problems, some novel electrical connectors need to be designed.

Chapter 3

System Modeling and Calibration

3.1 Single Joint Dynamics

A commonly used model for an n-dof of TLRLFJ model is introduced in [39] in the form of:

$$D(q_1)\ddot{q}_1 + C(q_1, \dot{q}_1) + k(q_1 - q_2) = 0 \tag{3.1}$$
$$J\ddot{q}_2 - k(q_1 - q_2) = u \tag{3.2}$$

Where $D(q_1)$ is n×n symmetric, positive definite inertial matrix. The vector $C(q_1, \dot{q}_1)$ contains coriolis, centripetal, friction and gravitational forces and torques. k and J are the n×n diagonal stiffness coefficients and motor inertial matrix, respectively. For the development of the decentralized control scheme, most approaches [48][26] are based on the above two equations and consider the inertial coupling term, the Coriolis, centrifugal, friction and gravity terms in (3.1) as disturbance torque.

A single joint module with harmonic drive (HD) can be modeled as a mass-spring system with three subsystems: 1) motor and wavegenerator (input) subsystem; 2) flexspline (transmission) subsystem; 3) link and load (output)subsystem; as shown in Fig. (3.1).By applying Euler-Lagrange theorem, three equations (3.3)(3.4)(3.5) can be derived for each subsystem. In this model, we assume the robot link moves in the vertical plan to count for more disturbance coming from the gravity of the link and unknown load.
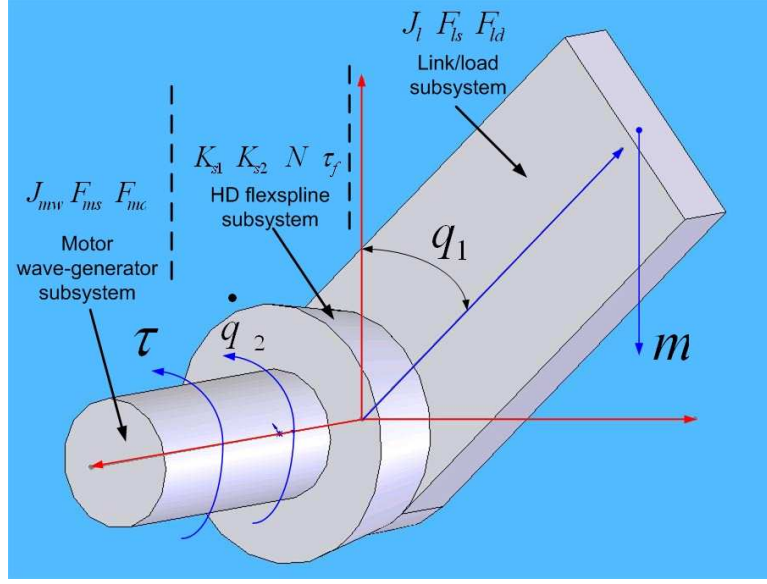
Figure 3.1: Joint schematics

$$J_{mw}\ddot{q}_2 + F_{md}\dot{q}_2 + F_{ms}sign(\dot{q}_2) + N\tau_f \quad = \quad \tau \qquad (3.3)$$

$$K_{s1}(Nq_2 - q_1) + K_{s2}(Nq_2 - q_1)^3 \quad = \quad \tau_f \qquad (3.4)$$

$$J_l\ddot{q}_1 + mglsin(q_1) + (F_{ld}\dot{q}_1 + F_{ls}sign(\dot{q}_1)) + \tau_d - \tau_f \quad = \quad 0 \qquad (3.5)$$

In equation (3.4)the compliance of the flexspline is modeled as a non-linear cubic function [27][53]. Substituting (3.5) into (3.3)(3.4) yields two equations representing the single joint dynamics:

$$\tau \quad = \quad J_{mw}\ddot{q}_2 + F_{md}\dot{q}_2 + F_{ms}sign(\dot{q}_2) + NK_{s1}(Nq_2 - q_1) + NK_{s2}(Nq_2 - q_1)^3 \qquad (3.6)$$

$$0 \quad = \quad J_l\ddot{q}_1 + mgl\sin(q_1) + F_{ld}\dot{q}_1 + F_{ls}sign(\dot{q}_1) - K_{s1}(Nq_2 - q_1) - K_{s2}(Nq_2 - q_1)^3 + \tau_d$$

$$(3.7)$$

Below are the definition of the variables/constants in equation (3.6)(3.7):

J_{mw} - motor rotor and HD wave-generator inertial

F_{md}, F_{ms} - input dynamic and static friction coefficients

K_{s1}, K_{s2} - flexspline stiffness coefficients

q_2, $\dot{q}_2$, $\ddot{q}_2$ - motor position, velocity and acceleration

N - HD gear reduction ratio

τ - motor input torque

J_l - output side inertia (link, load)

m - link gravity

l - link length

F_{ld}, F_{ls} - output side dynamic and static friction coefficients

q_1, $\dot{q}_1$, $\ddot{q}_1$ - link position, velocity and acceleration

τ_d - disturbance torque

The block diagram of the single joint dynamics in equation (3.6) and (3.7)is shown in Fig. (3.2).
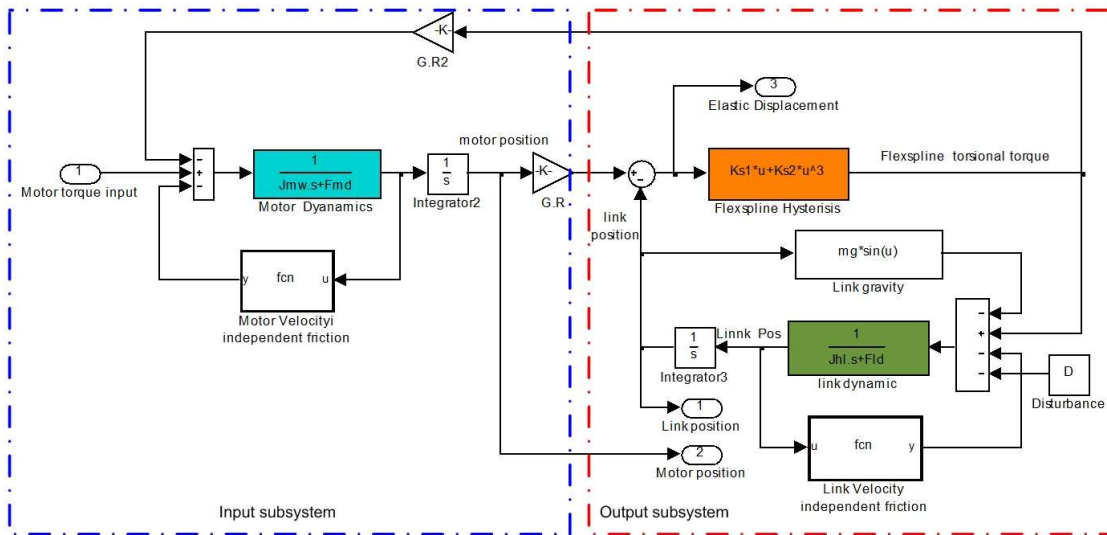
Figure 3.2: Block diagram of single joint model

The advantages of using the above decoupled dynamics are: 1) it is simpler in terms of computation compared with centralized controller because of the elimination of the

matrix manipulation; 2) less modifications are needed when the configuration is changed. For example, the matrices of $D(q_1)$ and $C(q_1, \dot{q}_1)$ in equation (3.1) express the inertial characteristics of the manipulator and they are configuration-dependent parameters. But the decoupled model eliminates the need to generate new $D(q_1)$ and $C(q_1, \dot{q}_1)$ for every new configuration.

3.1.1   Input Subsystem

The input subsystem consists of motor and HD wave-generator. Based on Euler-Lagrange equation, we have:

- Kinetic energy: $K = \frac{1}{2} J_{mw} \dot{q}_2^2$;

- Potential energy: $P = 0$;

- Lagrangian: $L = K - P = \frac{1}{2} J_{mw} \dot{q}_2^2$;

Therefore, the resulting torque can be calculated as:

$$\tau_m = \frac{d}{dt} \frac{\partial L}{\partial \dot{q}_2} - \frac{\partial L}{\partial q_2} = J_{mw} \ddot{q}_2 \tag{3.8}$$

This resulting torque τ_m is also related to motor input torque τ, friction torque and flexspline stiffness torque exerted on the input side. The following equation is satisfied:

$$\tau_m = \tau - (F_{md} \dot{q}_2 + F_{ms} sign(\dot{q}_2)) - N\tau_f \tag{3.9}$$

Therefore, the input subsystem dynamic equation is:

$$J_{mw} \ddot{q}_2 + F_{md} \dot{q}_2 + F_{ms} sign(\dot{q}_2) + N\tau_f = \tau \tag{3.10}$$

3.1.2   Transmission Subsystem

The transmission subsystem refers to flexible HD flexspline which usually runs at low speed, and its mass can be ignored. Therefore, we can model flexspline dynamic as a non-linear spring system [28] which generates torsional torque in the form of:

$$\tau_f = K_{s1}(Nq_2 - q_2) + K_{s2}(Nq_2 - q_1)^3 \tag{3.11}$$

3.1.3 Output Subsystem

The link and load are considered as the output subsystem. The link generates great effects on the robot dynamics. In our model, we assume the link mass m is exerted at the end of the link together with unknown load as shown in Fig. (3.1). Based on the Euler-Lagrange equation:

- Kinetic energy: $K = \frac{1}{2}J_l\dot{q}_1^2$;

- Potential energy: $P = -mgl\cos(q_1)$;

- Lagrangian: $L = K - P = \frac{1}{2}J_l\dot{q}_1^2 + mgl\cos(q_1)$;

The resulting torque is:

$$\tau_l = \frac{d}{dt}\frac{\partial L}{\partial \dot{q}_l} - \frac{\partial L}{\partial q_1} = J_l\ddot{q}_1 + mgl\sin(q_1) \tag{3.12}$$

The resulting torque τ_l is coming from the torsional torque applied by the flexspline, friction torque and disturbance, which can be expressed as:

$$\tau_l = \tau_f - (F_{ld}\dot{q}_1 + F_{ls}sign(\dot{q}_1)) - \tau_d \tag{3.13}$$

So the output dynamics is

$$J_l\ddot{q}_1 + mglsing(q_1) + (F_{ld}\dot{q}_1 + F_{ls}sign(\dot{q}_1) + \tau_d - \tau_f = 0 \tag{3.14}$$

Finally, we can rearrange (3.10)(3.11)(3.14) into two equation representing the single joint dynamics in (3.6) and (3.7).

3.2 MRR Transmission System Calibration

In order to precisely control such a system presented in equation (3.6) and (3.7), the flexspline stiffness coefficients K_{s1} and K_{s2}, and the output side dynamic and static friction coefficients F_{ld} and F_{ls} should be calculated accurately. The input dynamic and static friction F_{md}, F_{ms} can be found from motor manual provided by the manufacturer (Danaher Motion). The other parameters can be calculated based on he joint mechanical properties. The experiments setup and results are shown in the following subsections.

3.2.1 Harmonic Drive Flexspline Compliance

Fig. (3.3) and (3.4)shows the experimental setup for calibrating HD flexspline compliance. In this experiemnt, a CSF-32-100 HD is used. A brushless DC motor with an encoder (encoder A) monitoring the motor shaft position is coupled with the HD wave-generator. A Delta type force/torque (F/T) sensor is connected to the HD flexspline to record the applied torque and a high resolution encoder (encoder B) is mounted on the other side of F/T sensor to measure the output side displacement under certain load. The displacement of F/T sensor, provided by the manufacturer, is deducted from the encoder B's reading, and the coupling is assumed to be rigid. During the experiment, the motor is disenergized with the brake holding the motor shaft. In this case, the reading from encoder A is zero. Therefore, the flexspline torsion is the encoder B's reading. The dots in Fig. (3.5) are the experimental data of the flexspline torsion under certain applied load, and the solid curve is the fitted stiffness profile. The derived stiffness coefficients are the slope of the polyfit curve:

- $K_{s1} = 4 \times 10^4 Nm/rad$

- $K_{s2} = 2.5 \times 10^4 Nm/rad^3$

3.2.2 Harmonic Drive Flexspline Friction

The Coulomb and viscous friction can be identified by measuring the torque required to operate the HD at several different constant velocities. Instead of measuring the torque directly, we monitored the current flowing to the motor and multiplied it by torque constant.
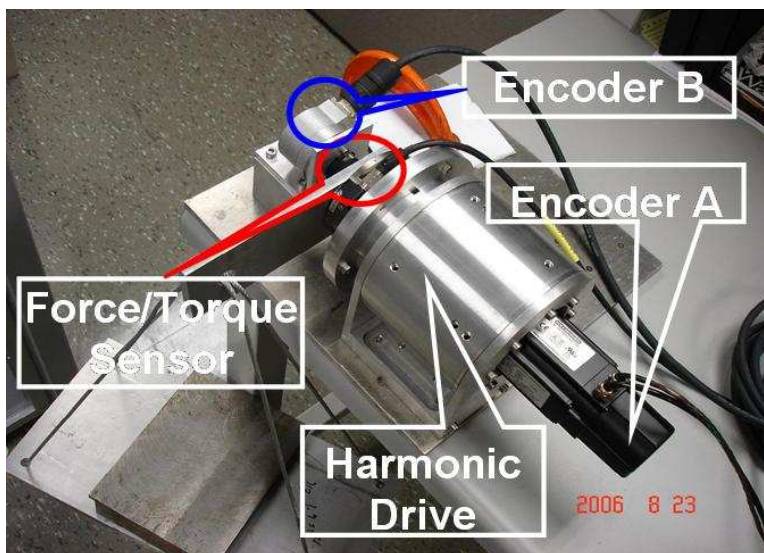
Figure 3.3: Experimental setup for HD flexspline compliance calibration (a)
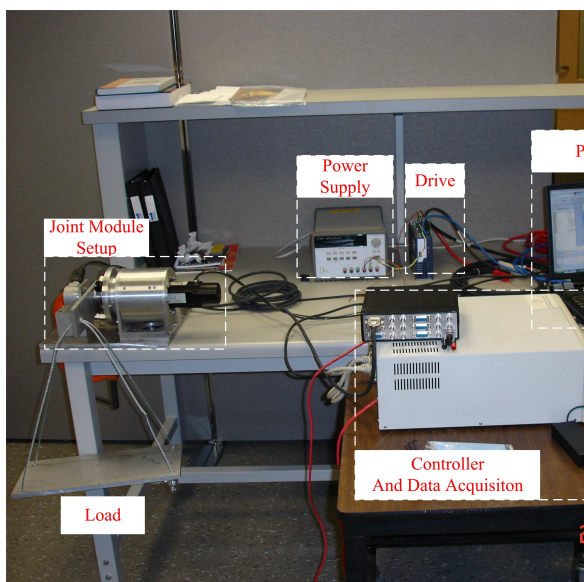
Figure 3.4: Experimental setup for HD flexspline compliance calibration (b)
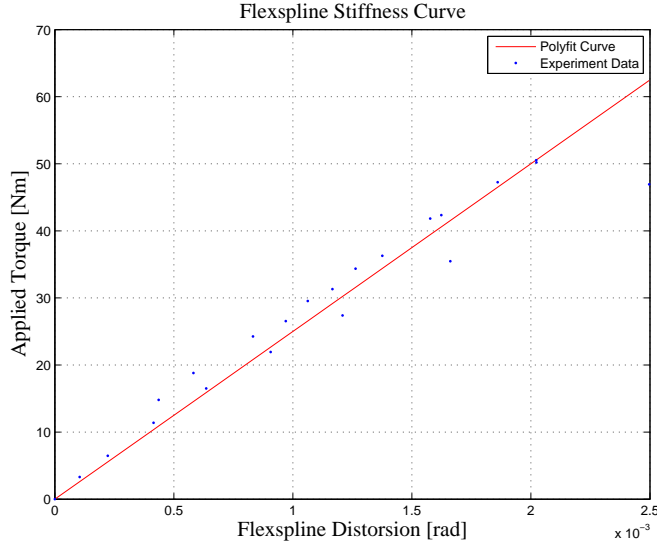
Figure 3.5: Flexspline stiffness experimental data and curve fitting

The dots in Fig. (3.6) is the experimental data. Obviously, a curve may fit properly, but based on literatures [27], the friction has a linear relationship with the velocity. Therefore, a line is fitted to the experimental data, as shown in Fig. (3.6). The slope of the line is the velocity-dependent viscous friction coefficient. The velocity-independent Coulomb friction coefficient is the friction torque at zero velocity. From the fitted line, we have:

- $K_{ld} = 0.226Nm$

- $K_{ls} = 0.0187Nm$

The stiffness and friction coefficients identified experimentally can be used to design the decentralized controller for the MRR.

3.3 Discussion

Robot manipulators exhibit nonlinear dynamics. In addition to unmodeled dynamics, due to varying payloads, gravitational effects and dynamic coupling between movements of
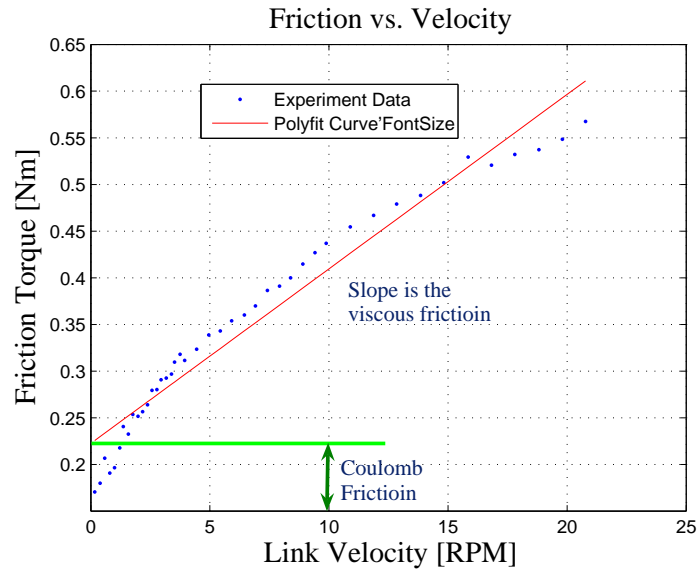
Figure 3.6: Harmonic drive friction experimental data and curve fitting

joints, the uncertainties due to friction and compliance of the HD transmission system, and dynamic parameters changes of the robot itself due to reconfiguration are also significant. To capture dynamic parameters, experiments were setup to estimate the HD friction and stiffness coefficients. Those coefficients will be used in chapter 4 to develop the control for the MRR. To avoid calculating new $D(q_1)$ and $C(q_1, \dot{q}_1)$ in equation (3.6) and (3.7), which are configuration-dependent parameters, we decoupled the MRR system and considered the single joint dynamics in control design. In this model, the coupling dynamic effects of the successive joints/joints are considered external disturbance [18].

Chapter 4

Controller Design

The objective of control design is to compensate for system dynamics so that the closed-loop system under the designed control has the desired performance. Loosely speaking, dynamic compensation is achieved by choosing a suitable control law to cancel the unexpected part of system dynamics. Feedback linearization control can achieve perfect cancelation for most dynamic systems, but a robotic system whose dynamics are inherently nonlinear. Nonlinear controller is definitely able to compensate for more uncertainties than linear controller.

Frequently changing configurations to cope with different tasks is the advantage of the modular and reconfigurable robot (MRR), but with the reconfiguration, the robot dynamics parameters also change. Therefore, controllers designed based on one configuration dynamics will not work well when the MRR is reconfigured. This is the reason why decentralized control technique is applied in our research. For decentralized control, each joint is considered as an independent subsystem, and the dynamic effects from the other links and joints are treated as disturbance. Therefore, the decentralized control is suitable for independent robot configurations so as to achieve modularity in software.

Due to significant uncertainties existing in the MRR dynamics, robust control is the better choice. Robust control is used to control unknown plants with unknown dynamics subject to unknown disturbances [54]. Some design tools and techniques have been developed for robust control are:

- **Lyapunov** - This is claimed to be the only universal technique for assessing non-

linear systems, which is based on stability analysis. The following section provides the basic concept of this technique.

- **Fuzzy logic** - Fuzzy logic is applicable to robust control because it is a method of handling uncertainties of the system. The technique is based upon the construction of fuzzy sets to describe the uncertainties inherent in all variables. The detailed information on designing this type of control and examples can be found in [56].

In this chapter, we designed a decentralized robust controller. Before introduced the detailed design process, we need to review two important techniques which were used in the controller development, they are : direct-Lyapunov method and integrator backstepping technique.

4.1 Direct-Lyapunov Method

Lyapunov stability theory plays a key role in analyzing and designing a nonlinear control system. The key point of the direct-Lyapunov method is to select an energy-like function, the so-called Lyapunov function, to study the behavior of the dynamic systems. The Lyapunov function is mathematically defined as a positive definite function. The time derivative of the energy-like function should be either negative or seminegative, which means the defined energy keeps dissipating. The definition of different stability, i.e. uniformly stable, uniformly asymptotically stable, etc. can be found in [57][58] [43].

Selecting a proper Lyapunov function for the specific dynamic system is the main task of the stability analysis. For robot manipulator systems, the following Lyapunov function is commonly selected:

$$V = \frac{1}{2}ke^2 + \frac{1}{2}\dot{e}^2 \tag{4.1}$$

where k is constant parameter, e is the robot position error, and $\dot{e}$ is the velocity error. The design objective is to select k and other control parameters to guarantee that the time derivative of the Lyapunov function V is negative or seminegaive, so that the robot dynamical system is proved to be stable.

4.2   Integrator Backstepping Techniques

Integrator backstepping technique has been widely used in robotics manipulators, autonomous underwater vehicles (AUV), etc. to achieve desired control objectives. We applied this technique in our robust controller design. In order to fully understand this concept, a brief introduction is presented in this subsection by giving an example from [58].

Suppose we have a system represented by the following dynamics as shown in equation (4.2).

$$\dot{q} = f(q) + g(q)p \tag{4.2}$$
$$\dot{p} = u \tag{4.3}$$

Where $[q, p]^T$ is the state and u is the control input.

The system dynamics can be represented by two subsystem as shown in Fig. (4.1). The objective is to design a state feedback controller to stabilize system at the operating point. The design steps are as follows:
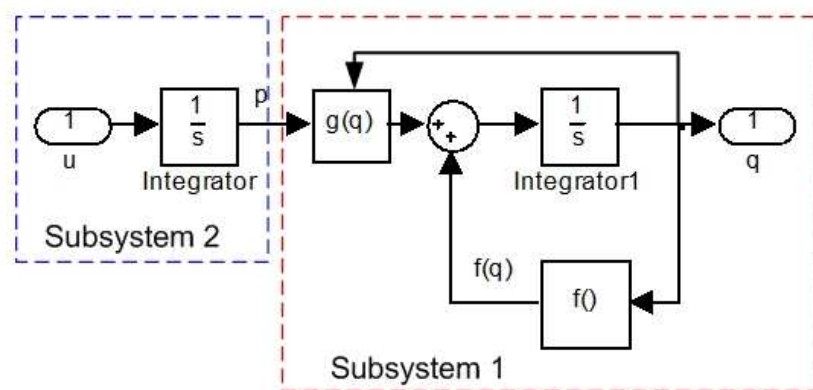
Figure 4.1: Backstepping: supposed system dynamics

Step 1:

Notice that the input of the first subsystem p is not the system control signal. This signal is not physically controllable. In order to stabilize this subsystem, we can rewrite equation (4.2) into the following form:

$$\dot{q} = [f(q) + g(q)h(q)] + g(q)[p - h(q)] \tag{4.4}$$
$$\dot{p} = u \tag{4.5}$$

The equivalent block diagram of the system is shown in Fig. (4.2).
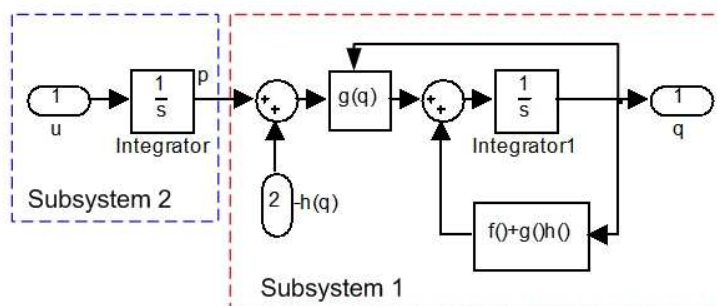
Figure 4.2: Backstepping: supposed system dynamics equivalent representation

Step 2:
The change of variables $z = p - h(q)$ results in the system

$$\dot{q} = [f(q) + g(q)h(q)] + g(q)z \tag{4.6}$$
$$\dot{z} = u - \dot{h} \tag{4.7}$$

This is referred to as backstep $-h(q)$ through the integrator as shown in Fig. (4.3).
  Step 3:
Selecting control law for both $h(q)$ and u to ensure the system stable and achieve the control objective.
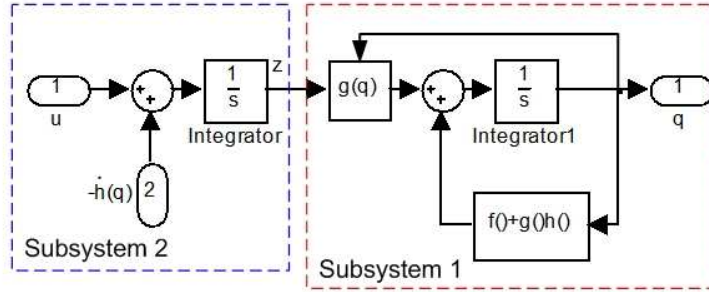
Figure 4.3: Backstepping: supposed system dynamics after integrator backstepping

4.3   Controller Design

As shown in the joint model block diagram (Fig. (3.2)), the dynamic system consists of two cascaded subsystems representing motor dynamics (3.6) and robot dynamics (3.7), respectively. The first subsystem of motor dynamics has the input τ, the motor control torque, and outputs, $q_2, \dot{q}_2$ and $\ddot{q}_2$, the motor states. The motor position q_2 is considered as the input to the second subsystem of robot dynamics which outputs $q_1, \dot{q}_1$ and $\ddot{q}_1$, the link states. The robot control signal q_2 is not the control signal that is sent to the system. In this situation, the backstepping method has to be used, and the robot input signal q_2 is called fictitious control signal [43]. The motor or system input signal τ is called system control signal. In order to design the system control signal τ, the fictitious control signal needs to be selected first, then stepped back to system control signal. Both fictitious control and system control signal are designed based on Lyapunov direct method. The proposed control law consists two terms: 1) a linear PD control, and 2) a nonlinear term to compensate for disturbances to the system.

In order for controller development, we introduce the following preliminary definitions

[43] made on parameters in equations (3.6) and (3.7).

$$Inertia \quad : \quad 0 < J < \widetilde{J} \tag{4.8}$$

$$Friction \quad : \quad \| F_s(\dot{q}) + F_d\dot{q} \| \leq F_1 + F_2 \| \dot{q} \| \tag{4.9}$$

$$Flexibility \quad : \quad 0 < K_i < \widetilde{K_i} \tag{4.10}$$

$$Disturbance \quad : \quad 0 < \| \tau \| < \widetilde{\tau} \tag{4.11}$$

Where $\widetilde{J}$ and $\widetilde{K_i}$ present the largest motor/link inertia and the largest stiffness coefficients of the MRR, respectively. $\widetilde{\tau}$ is the maximum disturbance.

4.3.1 Fictitious Control Law Selection

Suppose that the manipulator joint is required to track a desired joint angle q_1^d which has at least third order differentiability so that the desired velocity $\dot{q}_1^d$ and desired acceleration $\ddot{q}_1^d$ exist and can be derived from the derivative of q_1^d. The link error dynamics are calculated by adding $J_l\ddot{q}_1^d$ on both sides of (3.7), and after some simple manipulation, the link error dynamics can be formed as:

$$\begin{aligned} \ddot{e}_1 \quad = \quad & \ddot{q}_1^d + (J_l)^{-1}[F_{ld}\dot{q}_1 + F_{ls}sign(\dot{q}_1) + mgl\sin(q_1) \\ & +K_{s1}q_1 - K_{s2}(Nq_2 - q_1)^3 + \tau_d - K_{s1}Nq_2] \end{aligned} \tag{4.12}$$

Let

$$f(\dot{q}_1, q_1, q_2) \quad = \quad F_{ld}\dot{q}_1 + F_{ls}sign(\dot{q}_1) + mgl\sin(q_1) + K_{s1}q_1 - K_{s2}(Nq_2 - q_1)^3 + \tau_d \tag{4.13}$$

So equation (4.12) can be simplified as:

$$\ddot{e}_1 = \ddot{q}_1^d + (J_l)^{-1}[f(\dot{q}_1, q_1, q_2) - K_{s1}Nq_2] \tag{4.14}$$

The function $f(\dot{q}_1, q_1, q_2)$ includes all the uncertainties of the link dynamics,i.e. friction, stiffness and load disturbance. Based on assumptions made in equation (4.8) - (4.11), the

bounded uncertainty can be calculated:

$$
\begin{aligned}
f(\dot{q}_1, q_1, q_2) &= F_{ls} sign(\dot{q}_1) + mgl \sin(q_1) + \tau_d + K_{s1} q_1 + F_{ld} \dot{q}_1 - K_{s2}(N q_2 - q_1)^3 \\
&\leq F_{ls} + mgl + \tau_d + K_{s1} q_1 + F_{ld} \dot{q}_1 - K_{s2}(N q_2 - q_1)^3 \\
&= K_{10} + K_{11} q_1 + K_{12} \dot{q}_1 - K_{13}(N q_2 - q_1)^3 \\
&\equiv \Delta f
\end{aligned}
\tag{4.15}
$$

$$
\| \Delta f \| \leq K_{10} + K_{11} \| q_1 \| + K_{12} \| \dot{q}_1 \| + K_{13} \| (N q_2 - q_1)^3 \| \equiv \rho
\tag{4.16}
$$

The fictitious control signal q_2 in (4.14) can be chosen in the following form [43]:

$$
q_2 = \frac{J_l}{K_{s1} N}(\ddot{q}_1^d + K_1 e_1 + K_2 \dot{e}_1) + \frac{1}{K_{s1} N} \mu_r
\tag{4.17}
$$

Where $K_{s1} \neq 0$, $K_1 > 0$ and $K_2 > 0$ are linear PD control gains, and μ_r is an additional term designed to compensate the nonlinear uncertainties. Substitute (4.17) into (4.14), and the closed loop link error dynamics are:

$$
\ddot{e}_1 = -K_1 e_1 - K_2 \dot{e}_1 + (J_l)^{-1}(f(\dot{q}_1, q_1, q_2) - \mu_r)
\tag{4.18}
$$

To find the nonlinear term μ_r, the following Lyapunov function candidate is considered [43]:

$$
V_1' = \frac{1}{2} K_1 e_1^2 + \frac{1}{2} \dot{e}_1^2
\tag{4.19}
$$

Clearly, it is positive definite, and K_1 is the same PD control gain as shown in (4.17). Take the derivative on both sides and substitute (4.18) into it, we can have:

$$
\begin{aligned}
\dot{V}_1' &= K_1 e_1 \dot{e}_1 + \dot{e}_1 \ddot{e}_1 \\
&= K_1 e_1 \dot{e}_1 + \dot{e}_1(-K_1 e_1 - K_2 \dot{e}_1 + (J_l)^{-1}(f - \mu_r)) \\
&= -K_2 \| \dot{e}_1 \|^2 + (J_1)^{-1} \dot{e}_1 (f - \mu_r) \\
&\leq -K_2 \| \dot{e}_1 \|^2 + (J_1)^{-1} \dot{e}_1 (\Delta f - \mu_r)
\end{aligned}
\tag{4.20}
$$

If we select $\mu_r = \Delta f$, $\dot{V}_1' \leq 0$ is guaranteed. Therefore, the fictitious control law is:

$$
q_2 = \frac{J_l}{K_{s1} N}(\ddot{q}_1^d + K_1 e_1 + K_2 \dot{e}_1) + \frac{1}{K_{s1} N} \Delta f \equiv \phi
\tag{4.21}
$$

Equation (4.21) represents the fictitious control law, whcih is a saturation type control [44] because the nonlinear term Δf is bounded.

4.3.2 Backstepping

The fictitious control law has been selected, but it needs to be backstepped to the side of the motor dynamics subsystem. To do so, we can add and subtract $(J_l)^{-1}K_{s1}N\phi$ to the right side of (4.14), where ϕ denotes the fictitious control variable:

$$\ddot{e}_1 = \ddot{q}_1^d + (J_l)^{-1}[f - K_{s1}N\phi] - (J_l)^{-1}K_{s1}N(q_2 - \phi) \tag{4.22}$$

Equations (4.22) and (3.6) form the new dynamics of the single joint. If $q_2 - \phi = 0$, the equation (4.22) is stable, since ϕ is a robust controller, which is shown above. Therefore, out goal is to design robust control law τ in equation (3.6) such that $q_2 - \phi$ either converges to zero or at least is bounded by a constant. The following Lyapunov candidate for he overall system is used [43]:

$$
\begin{aligned}
V &= V_1 + V_2 + V_3 \\
&= [\frac{1}{2}K_1 e_1^2 + \frac{1}{2}(\dot{e}_1)^2] + [\frac{1}{2}K_3 e_2^2 + \frac{1}{2}(\dot{e}_2)^2] + \frac{1}{2}(q_2 - \phi)^2
\end{aligned}
\tag{4.23}
$$

Where $K_3 > 0$ is another PD controller gain which will be defined later. Replacing $\ddot{e}_1$ by new error dynamics (4.22) and substitute the fictitious control ϕ, we have:

$$
\begin{aligned}
\dot{V}_1 &= K_1 e_1 \dot{e}_1 + \dot{e}_1 \ddot{e}_1 \\
&= K_1 e_1 \dot{e}_1 + \dot{e}_1(\ddot{q}_1^d + (J_l)^{-1}[f - K_{s1}N\phi] - (J_l)^{-1}K_{s1}N(q_2 - \phi)) \\
&= K_1 e_1 \dot{e}_1 + \dot{e}_1\{\ddot{q}_1^d + (J_l)^{-1}[f - K_{s1}N(\frac{J_l}{K_{s1}N}[\ddot{q}_1^d + K_1 e_1 + K_2 \dot{e}_1] + \frac{1}{K_{s1}N}\Delta f)]\} \\
&\quad -(J_1)^{-1}K_{s1}N\dot{e}_1(q_2 - \phi) \\
&= K_1 e_1 \dot{e}_1 + \dot{e}_1(-K_1 e_1 - K_2 \dot{e}_1) + (J_l)^{-1}\dot{e}_1(f - \Delta f) - (J_l)^{-1}K_{s1}N\dot{e}_1(q_2 - \phi) \\
&\leq -K_2 \parallel \dot{e}_1 \parallel^2 -(J_l)^{-1}K_{s1}N\dot{e}_1(q_2 - \phi)
\end{aligned}
\tag{4.24}
$$

In order to calculate the derivative of V_2, the motor error dynamics need to be formed. Add $J_{mw}\ddot{q}_2^d$ to both sides of (3.6) and perform some simple manipulation, we have:

$$
\begin{aligned}
J_{mw}(\ddot{q}_2^d - \ddot{q}_2) &= J_{mw}\ddot{q}_2^d + F_{md}\dot{q}_2 + F_{ms}sign(\dot{q}_2) + NK_{s1}(Nq_2 - q_1) + NK_{s2}(Nq_2 - q_1)^3 - \tau \\
\ddot{e}_2 &= \ddot{q}_2^d + J_{mw}^{-1}[g(\dot{q}_2, q_2, q_1) - \tau]
\end{aligned}
\tag{4.25}
$$

Similar to $f(\dot{q}_1, q_1, q_2)$ in (4.16), $g(\dot{q}_2, q_2, q_1)$ contains all the uncertainties of the motor dynamic subsystem, i.e. motor rotor friction, flexspline compliance, and the upper bounded function is defined as:

$$g(\dot{q}_2, q_2, q_1) = F_{md}\dot{q}_2 + F_{ms}sign(\dot{q}_2) + NK_{s1}(Nq_2 - q_1) + NK_{s2}(Nq_2 - q_1)^3$$

(4.26)

$$\| g(\dot{q}_2, q_2, q_1) \| \leq K_{20} + K_{21} \| \dot{q}_2 \| + K_{22} \| (Nq_2 - q_1) \| + K_{23} \| (Nq_2 - q_1)^3 \|$$
$$\equiv \beta$$

(4.27)

Similar to the fictitious control law in (4.17), the control signal τ can be chosen as [43]:

$$\tau = J_{mw}(\ddot{q}_2^d + K_3 e_2 + K_4 \dot{e}_2) + u_1$$

(4.28)

Where $K_3 > 0$ and $K_4 > 0$ are the linear PD gains, and u_1 is nonlinear term to guarantee $\dot{V} \leq 0$ while not $\dot{V}_2 \leq 0$ itself. Take the derivative of V_2, and substitute (4.25), (4.26) and (4.28), we have:

$$
\begin{aligned}
\dot{V}_2 &= K_3 e_2 \dot{e}_2 + \dot{e}_2 \ddot{e}_2 \\
&= K_3 e_2 \dot{e}_2 + \dot{e}_2(\ddot{q}_2^d + J_{mw}^{-1}(g - \tau)) \\
&= K_3 e_2 \dot{e}_2 + \dot{e}_2\{\ddot{q}_2^d + J_{mw}^{-1}[g - J_{mw}(\ddot{q}_2^d + K_3 e_2 + K_4 \dot{e}_2) - u_1]\} \\
&\leq K_3 e_2 \dot{e}_2 + \dot{e}_2(-K_3 e_2 - K_4 \dot{e}_2) + J_{mw}^{-1} \dot{e}_2(\beta - u_1) \\
&= -K_4 \| \dot{e}_2 \|^2 + J_{mw}^{-1}(\beta - u_1)
\end{aligned}
$$

(4.29)

Finding $\dot{V}_3$ is not a straightforward task, because V_3 in (4.23) is a function of fictitious control law ϕ in (4.21), which is a function of desired link acceleration, link position error, link velocity error and bounded function ρ. Therefore, the derivative of V_3 introduces link acceleration error which is very difficult to measure. The following calculation is targeted to eliminate the link acceleration error term.

We can consider the simple form of $\dot{V}_3$

$$\dot{V}_3 = (q_2 - \phi)(\dot{q}_2 - \dot{\phi})$$

(4.30)

$\dot{V}$ can be formed by combining (4.29), (4.30) and (4.24), that is:

$$
\begin{aligned}
\dot{V} \ \leq \ & -K_2 \parallel \dot{e}_1 \parallel^2 -(J_l)^{-1} K_{s1} N \dot{e}_1 (q_2 - \phi) - K_4 \parallel \dot{e}_2 \parallel^2 + J_{mw}^{-1} \dot{e}_2 (\beta - u_1) \\
& + (q_2 - \phi)(\dot{q}_2 - \dot{\phi}) \\
= \ & -K_2 \parallel \dot{e}_1 \parallel^2 -K_4 \parallel \dot{e}_2 \parallel^2 + (q_2 - \phi)(\dot{q}_2 - \dot{\phi} - (J_l)^{-1} K_{s1} N \dot{e}_1) + J_{mw}^{-1} \dot{e}_2 \beta - J_{mw}^{-1} \dot{e}_2 u_1 \\
\leq \ & -K_2 \parallel \dot{e}_1 \parallel^2 -K_4 \parallel \dot{e}_2 \parallel^2 + \parallel q_2 - \phi \parallel (\parallel \dot{q}_2 \parallel + \parallel \dot{\phi} \parallel + (J_l)^{-1} K_{s1} N \parallel \dot{e}_1 \parallel) \\
& + J_{mw}^{-1} \parallel \dot{e}_2 \parallel \beta - J_{mw}^{-1} \dot{e}_2 u_1
\end{aligned}
\tag{4.31}
$$

To find u_1, $\dot{\phi}$ needs to be calculated first, from (4.21)

$$
\dot{\phi} = \frac{J_l}{K_{s1} N}(q_1^{d(3)} + K_1 \dot{e}_1 + K_2 \ddot{e}_1) + \frac{1}{K_{s1} N} \Delta \dot{f}
\tag{4.32}
$$

From (4.16) we can calculate $\dot{\rho}$

$$
\dot{\rho} = K_{11} \dot{q}_1 + K_{12} \ddot{q}_1 + 3 K_{13}(N q_2 - q_1)^2 (N \dot{q}_2 - \dot{q}_1)
\tag{4.33}
$$

Substitute (4.33) into (4.32)

$$
\begin{aligned}
\Delta \dot{f} \ = \ & \frac{J_l}{K_{s1} N}(q_1^{d(3)} + K_1 \dot{e}_1 + K_2 \ddot{e}_1) + \frac{1}{K_{s1} N}[K_{11} \dot{q}_1 + K_{12} \ddot{q}_1 + 3 K_{13}(N q_2 - q_1)^2 (N \dot{q}_2 - \dot{q}_1)] \\
= \ & \frac{J_l}{K_{s1} N}[q_1^{d(3)} + K_1 \dot{e}_1 + K_2 \ddot{e}_1] + \frac{1}{K_{s1} N} K_{11} \dot{q}_1 + \frac{1}{K_{s1} N} K_{12} \ddot{q}_1 \\
& + \frac{3}{K_{s1} N} K_{13}(N q_2 - q_1)^2 (N \dot{q}_2 - \dot{q}_1) \\
= \ & \frac{J_l}{K_{s1} N}[q_1^{d(3)} + K_1 \dot{e}_1 + K_2 \ddot{e}_1] + \frac{1}{K_{s1} N} K_{11} \dot{q}_1^d - \frac{1}{K_{s1} N} K_{11} \dot{e}_1 + \frac{1}{K_{s1} N} K_{12} \ddot{q}_1^d \\
& - \frac{1}{K_{s1} N} K_{12} \ddot{e}_1 + \frac{3}{K_{s1} N} K_{13}(N q_2 - q_1)^2 (N \dot{q}_2 - \dot{q}_1) \\
= \ & \frac{J_l}{K_{s1} N} q_1^{d(3)} + \frac{1}{K_{s1} N} K_{12} \ddot{q}_1^d + \frac{1}{K_{s1} N} K_{11} \dot{q}_1^d + \frac{3}{K_{s1} N} K_{13}(N q_2 - q_1)^2 (N \dot{q}_2 - \dot{q}_1) \\
& + \frac{1}{K_{s1} N}(J_l K_1 - K_{11}) \dot{e}_1 + \frac{1}{K_{s1} N}(J_l K_2 - K_{12}) \ddot{e}_1
\end{aligned}
$$

$$\tag{4.34}$$

Therefore,

$$
\begin{aligned}
\parallel \dot{\phi} \parallel \;\leq\;\; & \frac{J_l}{K_{s1}N} \parallel q_1^{d(3)} \parallel + \frac{1}{K_{s1}N}[K_{12} \parallel \ddot{q}_1^d \parallel + K_{11} \parallel \dot{q}_1^d \parallel] \\
& + \frac{3}{K_{s1}N} K_{13}(Nq_2 - q_1)^2 \parallel N\dot{q}_2 - \dot{q}_1 + \frac{1}{K_{s1}N} \parallel J_l K_1 - K_{11} \parallel \parallel \dot{e}_1 \parallel \\
& + \frac{1}{K_{s1}N} \parallel J_l K_2 - K_{12} \parallel \parallel \ddot{e}_1 \parallel \\
\leq\;\; & \frac{J_l}{K_{s1}N} \sup_{t\geq 0} \parallel q_1^{d(3)} \parallel + \frac{1}{K_{s1}N} K_{12} \sup_{t\geq 0} \parallel \ddot{q}_1^d \parallel + \frac{1}{K_{s1}N} K_{11} \sup_{t\geq 0} \parallel \dot{q}_1^d \parallel \\
& + \frac{3}{K_{s1}N} K_{13}(Nq_2 - q_1)^2 \parallel N\dot{q}_2 - \dot{q}_1 \parallel + \frac{1}{K_{s1}N} \parallel J_l K_1 - K_{11} \parallel \parallel \dot{e}_1 \parallel \\
& + \frac{1}{K_{s1}N} \parallel J_l K_2 - K_{12} \parallel \parallel \ddot{e}_1 \parallel \tag{4.35}
\end{aligned}
$$

The following observations can be made:

- If $J_l K_2 - K_{12} = 0$ is satisfied by choosing $K_2 = \frac{K_{12}}{J_l}$, $\ddot{e}_1$ can be eliminated.

- Because the flexspline elastic displacement is very small (e.g. in 10^{-4}rad range), which can be determined by experiments. Therefore, $\frac{3}{K_{s1}N} K_{13}(Nq_2 - q_1)^2 \parallel N\dot{q}_2 - \dot{q}_1 \parallel$ is small and bounded. Let

$$
\begin{aligned}
K_{30} \;\geq\;\; & \frac{1}{K_{s1}N}[J_l \sup_{t\geq 0} \parallel q_1^{d(3)} \parallel + K_{12} \sup_{t\geq 0} \parallel \ddot{q}_1^d \parallel + K_{11} \sup_{t\geq 0} \parallel \dot{q}_1^d \parallel] \\
& + \frac{3}{K_{s1}N}(Nq_2 - q_1)^2 \parallel N\dot{q}_2 - \dot{q}_1 \parallel
\end{aligned}
$$

- Let

$$
K_{31} \geq \frac{1}{K_{s1}N} \parallel J_l K_1 - K_{11} \parallel
$$

By applying the above observations to (4.35), we have:

$$
\parallel \dot{\phi} \parallel \leq K_{30} + K_{31} \parallel \dot{e}_1 \parallel \tag{4.36}
$$

Substitute (4.36) into (4.31), and consider $\| \dot{q}_2 \| \leq \| \dot{q}_2^d \| + \| \dot{e}_2 \|$, we have:

$$
\begin{aligned}
\dot{V} \leq & -K_2 \| \dot{e}_1 \|^2 -K_4 \| \dot{e}_2 \|^2 +J_{mw}^{-1} \| \dot{e}_2 \| \| \beta \| -J_{mw}^{-1}\dot{e}_2 u_1 \\
& + \| q_2 - \phi \| \{ \| \dot{q}_2^d \| + \| \dot{e}_2 \| +K_{30} + K_{31} \| \dot{e}_1 \| +(J_l)^{-1}K_{s1}N \| \dot{e}_1 \| \} \\
\leq & -K_2 \| \dot{e}_1 \|^2 -K_4 \| \dot{e}_2 \|^2 +J_{mw}^{-1} \| \dot{e}_2 \| \| \beta \| -J_{mw}^{-1}\dot{e}_2 u_1 \\
& + \| q_2 - \phi \| \{ (\sup_{t \geq 0} \| \dot{q}_2^d \| +K_{30}) + (K_{31} + (J_l)^{-1}K_{s1}N) \| \dot{e}_1 \| + \| \dot{e}_2 \| \}
\end{aligned}
$$
$$(4.37)$$

Ideally, $\| \dot{e}_1 \| = N \| \dot{e}_2 \|$, therfore we can find a K'_{31} to satisfy

$$
K'_{31} \| \dot{e}_2 \| \geq J_{mw}\{(K_{31} + (J_l)^{-1}K_{s1}N) \| \dot{e}_1 \| + \| \dot{e}_2 \| \} \tag{4.38}
$$

Let

$$
K'_{30} \geq J_{mw}(\sup_{t \geq 0} \| \dot{q}_2^d \| +K_{30}) \tag{4.39}
$$

Equation (4.37) can be simplified to:

$$
\begin{aligned}
\dot{V} \leq & -K_2 \| \dot{e}_1 \|^2 -K_4 \| \dot{e}_2 \|^2 +J_{mw}^{-1} \| q_2 - \phi \| (K'_{30} + K'_{31} \| e_2 \|) + J_{mw}^{-1} \| \dot{e}_2 \| \| \beta \| \\
& -J_{mw}^{-1}\dot{e}_2 u_1 \\
= & -K_2 \| \dot{e}_1 \|^2 -K_4 \| \dot{e}_2 \|^2 +J_{mw}^{-1}K'_{30} \| q_2 - \phi \| +J_{mw}^{-1}K'_{31} \| q_2 - \phi \| \| \dot{e}_2 \| \\
& +J_{mw}^{-1} \| \dot{e}_2 \| \| \beta \| -J_{mw}^{-1}\dot{e}_2 u_1
\end{aligned}
$$
$$(4.40)$$

We can choose nonlinear term u_1 in the form of

$$
u_1 = \frac{K_{33}\dot{e}_2}{\| \dot{e}_2 \| +K_{32}}(K'_{30} \| q_2 - \phi \| +K'_{31} \| q_2 - \phi \| + \| \beta \|) \tag{4.41}
$$

Substitute (4.41) into (4.40), the final $\dot{V}$ is

$$
\begin{aligned}
\dot{V} \leq & -K_2 \| \dot{e}_1 \|^2 -K_4 \| \dot{e}_2 \|^2 +J_{mw}^{-1}K'_{30} \| q_2 - \phi \| (1 - \frac{K_{33} \| \dot{e}_2 \|^2}{\| \dot{e}_2 \| +K_{32}}) \\
& +J_{mw}^{-1}(\| \dot{e}_2 \| -\frac{K_{33} \| \dot{e}_2 \|^2}{\| \dot{e}_2 \| +K_{32}})(K'_{31} \| q_2 - \phi \| + \| \beta \|) \\
\leq & -K_2 \| \dot{e}_1 \|^2 -K_4 \| \dot{e}_2 \|^2 +J_{mw}^{-1}K'_{30} \| q_2 - \phi \| (\frac{\| \dot{e}_2 \| +K_{32} - K_{33} \| \dot{e}_2 \|^2}{\| \dot{e}_2 \| +K_{32}}) \\
& +J_{mw}^{-1}(\frac{\| \dot{e}_2 \|^2 +K_{32} \| \dot{e}_2 \| -K_{33} \| \dot{e}_2 \|^2}{\| \dot{e}_2 \| +K_{32}})(K'_{31} \| q_2 - \phi \| + \| \beta \|)
\end{aligned}
$$
$$(4.42)$$

Because K_{32} and K_{33} are control parameters, we can choose suitable values to ensure

$$K_{33} \parallel \dot{e}_2 \parallel^2 \;\; \geq \;\; \parallel \dot{e}_2 \parallel +K_{32}$$
$$K_{33} \parallel \dot{e}_2 \parallel^2 \;\; \geq \;\; \parallel \dot{e}_2 \parallel^2 +K_{32} \parallel \dot{e}_2 \parallel$$

Therefore, we can achieve $\dot{V} \leq 0$. This implies uniformly ultimate bounded stability given the fact that K_{33} approaches infinity as e_2 approaches zero. Substitute (4.41) into (4.28), the final control torque is:

$$\tau \;\; = \;\; J_{mw}(\ddot{q}_2^d + K_3 e_2 + K_4 \dot{e}_2) + \frac{K_{33}\dot{e}_2}{\parallel \dot{e}_2 \parallel +K_{32}}(K_{30}' \parallel q_2 - \phi \parallel +K_{31}' \parallel q_2 - \phi \parallel + \parallel \beta \parallel)$$

$$(4.43)$$

For MRR, the configuration change presents a new set of robot dynamic parameters. Hence, decentralized control is a suitable strategy to handle motion tracking of MRR. In decentralized control, every joint is treated as a single input single output (SISO) system plus a disturbance torque representing all uncertainties of the robot. In equation (4.43), K_{33} and K_{32} are control parameters; K_{30}', K_{31} and β are determined based on the upper bound on the link/motor dynamics. Therefore, (4.43) does not directly depends on the link parameters and will require minimal (or no) change of control parameters when robot is reconfigured. The proposed control law is a saturation type controller because of the bounded nonlinear term u_1 in equation (4.28).

4.4 Discussion

In this chapter, a nonlinear decentralized robust controller was developed based on the derived joint dynamics model in chapter (3). The stability analysis was performed use direct-Lyapunov method and backstepping techniques. The robust controller is independent on the link/motor dynamics because of the deployment of the upper bound dynamics. In addition, we used a more accurate nonlinear model for the harmonic drive (HD) compliance. The controller validation is studied in the following chapter.

Chapter 5

Controller Validation

The proposed robust controller was validated by both computer simulation and experiments, which are presented in this chapter. The MRR robot designed in this research is still under development at the time of writing this thesis. Therefore, we conducted experiments using another MRR system that was built by Engineering Service Inc. (ESI), Toronto, Ontario. On the other hand, simulations were developed using parameters of the joint module in chapter 3 to give insight into the expected performance of the proposed MRR system.

5.1   Simulation

Matlab Simulink is used as a simulaiton tool to validate the proposed controller. The block diagram of a trajectory tracking system is shown in Fig. (5.1), which is generated based on equation (3.6) and (3.7). It primarily consists of a trajectory reference input, a robust controller which is separated as a linear controller and a nonlinear controller, and MRR joint dynamics.

In this simulation model, we assume that there is no processing, measurement and signal transmission noise, and all the MRR system uncertainties are included inside the joint block. In addition, the simulator considers the fact that the controller output signal τ is limited by the motor peak input torque.

Also, a velocity observer is used to estimate the motor/link velocity, demonstrating the

controller will function despite not having direct measurements of the motor/link velocity. A first-order, high-pass filter is deployed as an observer to estimate the velocity tracking error based on filtering techniques. The observer is in the following form [52]:

$$e_v = -ke_p + p \tag{5.1}$$

$$\dot{p} = -(k+1)p + (k^2+1)e_p \tag{5.2}$$

where, e_v and e_p are the velocity and position tracking error, respectively. k is positive constant scalar. p is an auxiliary variable introduced to permit implementation of the filter without utilizing velocity measurements. From the discrete time point of view, the status p at time k is updated based on the previous p and position error e_p at time $k-1$.
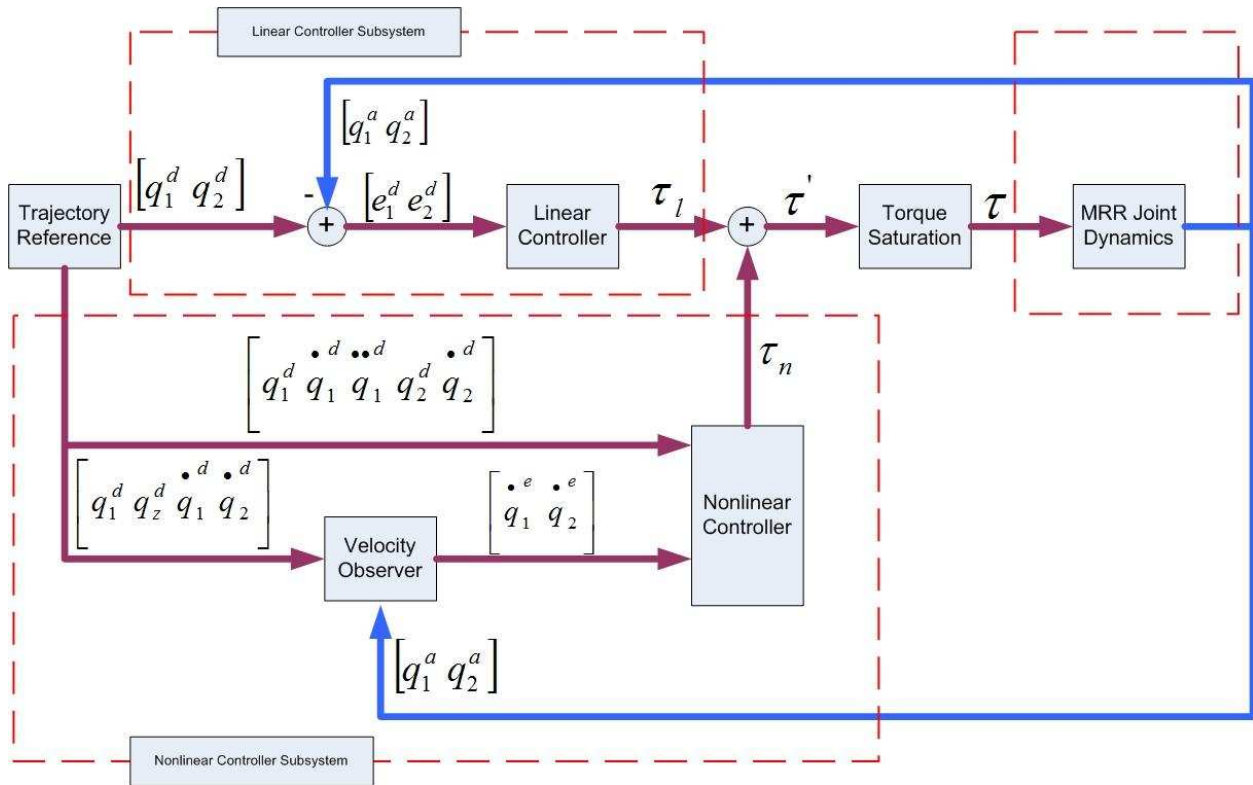

Figure 5.1: Robust controller simulink block diagram

5.1.1 Simulation Results

The single joint was simulated to follow a sinusoidal trajectory with a frequency of 1/20Hz and a amplitude of 90deg under two scenarios: without load and with 30lb (13.6kg) load. The position error, velocity error, controller output and flexspline displacement are shown below. From the results we can see both position error and velocity error are acceptable, but the error is larger for the case of with lad than that of without load. This is is because the load generates more disturbance to the system. Another observation is that the largest error occurs at the position where the joint changes its rotation direction, which also causes disturbances due to the link/load inertia dynamic effects.
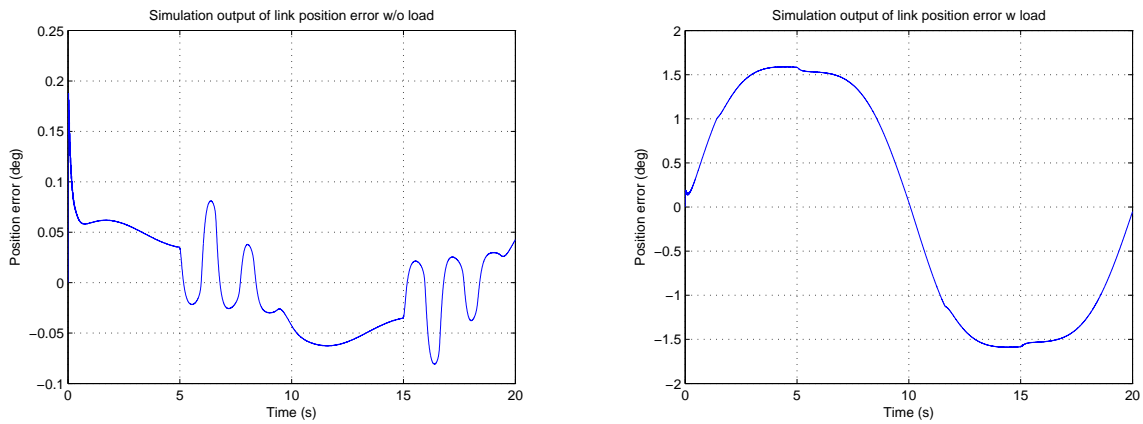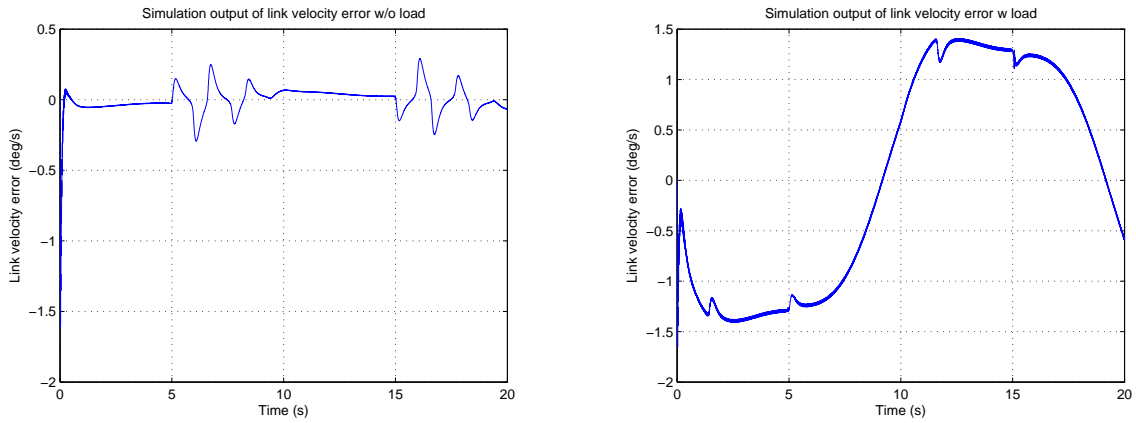

Figure 5.2: Position error with and without load

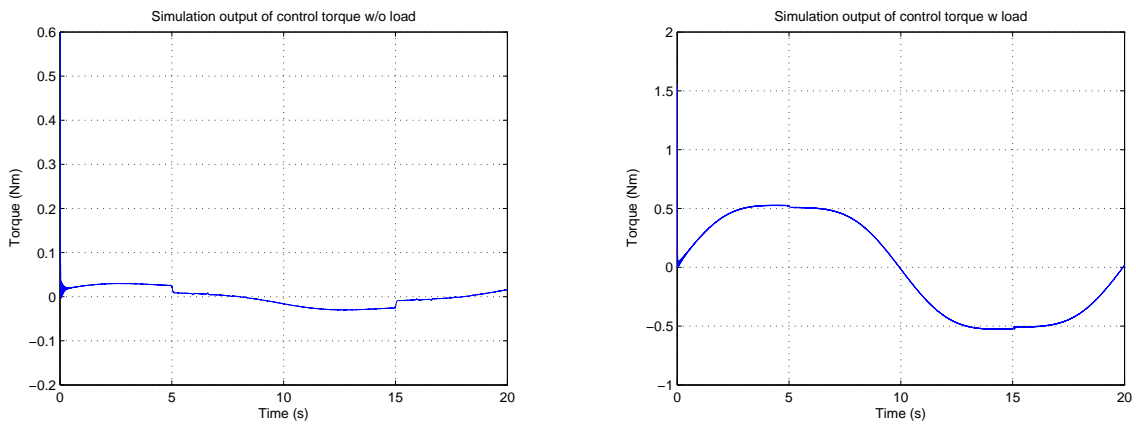Figure 5.3: Velocity error with and without load

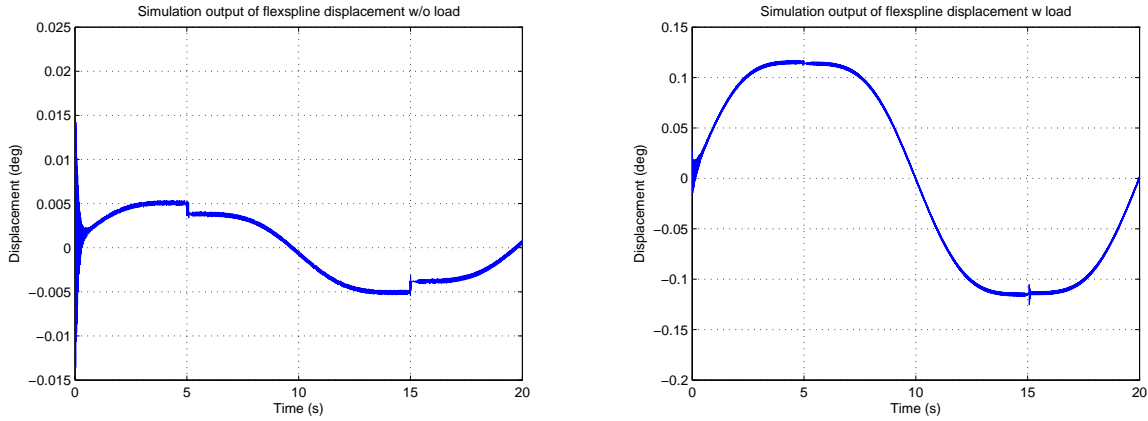Figure 5.4: Controller output with and without load

Figure 5.5: Flexspline displacement with and without load

5.2   Experiments Setup

The proposed robust controller was also validated experimentally,which was done on a modular and reconfigurable robot (MR) system that was built by the Engineering Service Inc., Toronto, Ontario. Fig. (5.6) shows the MRR, which has 4-DOF with a pneumatic gripper. Between the gripper and the last joint, there is a force and torque sensor. Each joint has two input ports and one output, so that can be reconfigured. Table (5.1) lists all kinematic parameters. In this table, the offsets are the distance "d" shown in Fig. (1.10), and the joint dimension is the cubic envelop of each joint. Joint operation range is measured with each single joint. The actual joint rotational range will be less than this value because of the interference among joints and links. The dynamic parameters are shown in table (5.2). In our experiments, we only controlled the first 3-DOf, and the last joint together with the griper and torque sensor were considered as load.

Fig. (5.7) shows the MRR system block diagram. The MRR is controlled by a MSK2812 DSP-based micro-controller via controller area network (CAN) communication bus. The DSP is connected to a desk top PC, on which the robust control algorithm is implemented in C language. The program is downloaded to the DSP through RS232. During execution, the control command is distributed to each joint module via CAN bus, and the feedback signals, i.e. position, velocity and torque, are also transmitted back to DSP via CAN bus
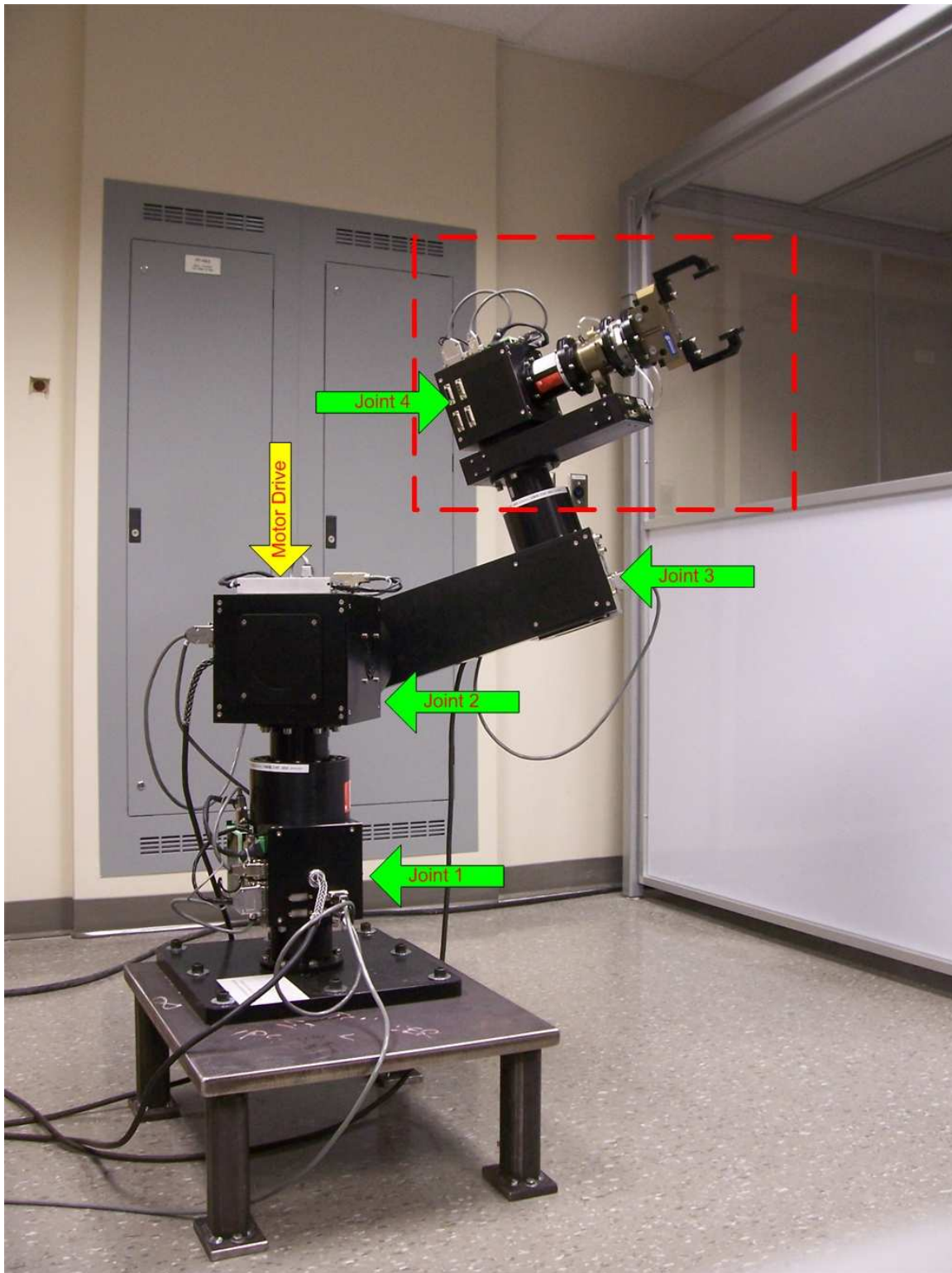
Figure 5.6: Modular and reconfigurable robot system built by ESI

Table 5.1: ESI MRR system kinematic parameters

ESI MRR kinematic parameters				
	Joint 1	Joint21	Joint 3	Joint43
Link length (mm)	430			
Offset (mm)	200	110	110	110
Joint dimension (mm)	198*216*370	152*168*310	152*168*310	152*168*310
Joint angle ranges (deg)	0-340	0-340	0-340	0-340

Table 5.2: ESI MRR system dynamic parameters

ESI MRR dynamic parameters				
	Joint 1	Joint21	Joint 3	Joint43
Link Inertia(mm)	0.11			
Rated output torque (Nm)	119.84	334.4	46.7	4.17
Rated speed (rpm)	39	24	75.5	102.5
HD reduction ratio	160	160	100	100

and stored into the memory block. All such data can be uploaded to PC offline for further analysis.

Figure 5.7: ESI MRR system block diagram

The three joints of the MRR were controlled to track the following trajectory:
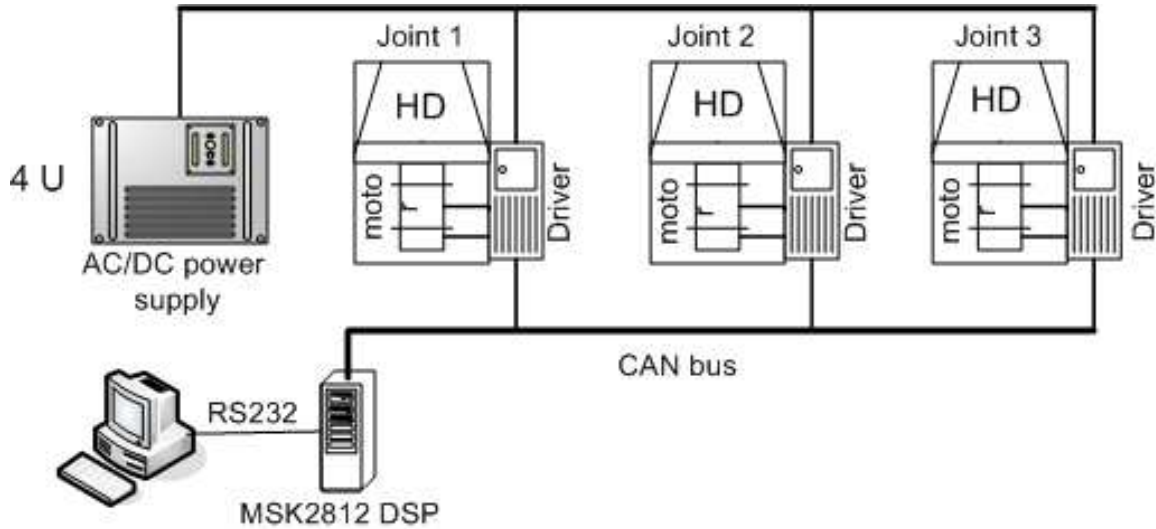
$$Traj \;=\; A\sin(\frac{2\pi}{T} * (\frac{j}{f})) \tag{5.3}$$

Where $A = 90deg$, is the trajectory amplitude, $T = 10s$ is the trajectory period, $f = 50Hz$ is the control frequency, and $j = 0, 1, ...$ is the control signal index.

The control frequency is limited by CAN bus data transmission rate. The MSK2812 DSP is operated at 150MHz, which has a powerful calculation capabilities, but the data transmission rate of the CAN bus is 1 Mbit/s. In each control cycle, the torque and other control commands, i.e. open/close brake, set correct operation mode, are sent to all three joints, the feedback signal from each joint is also transmitted back to controller. All those commands are either 32bits or 16bits, combining with other CAN frame headers, there is a considerable amount of data already being sent on the CAN bus. Hence only low control frequency (50Hz) is possible.

Fig. 5.8 shows the desired trajectory for all three joints. We did the test on two different MRR configurations, which are shown in Fig.(5.9) and Fig.(5.10), respectively. For each configuration, we controlled the robot without load and with load. Because we only control the first three joints, the last one was considered as load, as shown in Fig. (5.9). In Fig. (5.10), the third joint and link were not shown. We did ten trials for each scenarios. The experimental results are shown in the next subsection, followed by discussion.
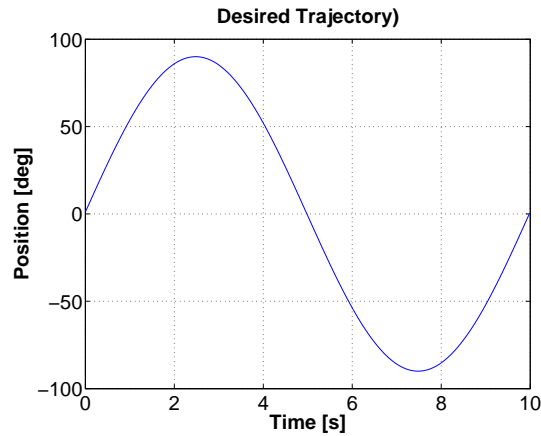
Figure 5.8: desired trajectory

5.2.1 Experimental Results

In this section we perform experimental analysis. Due to the limitation of DSP memory size, only one period of position and torque signals of each joint were captured, which are shown in Fig. (5.11)-Fig. (5.34).

The first set of experiments was performed on configuration 1 without load as shown in Fig. (5.9). In the experiments, we compared the performance of the proposed decentralized robust controller with that of PID controller. The results are shown in Fig. (5.11) - Fig.(5.16). For each comparison, we first show the position tracking error followed by the controller torque output. Using the same MRR configuration, we conducted the same experiments but with a load of 30 lb, and the results are shown in Fig. (5.17)-(5.22). We repeated same procedures on the second configuration, and the results are shown

Figure 5.9: configuration 1: with load
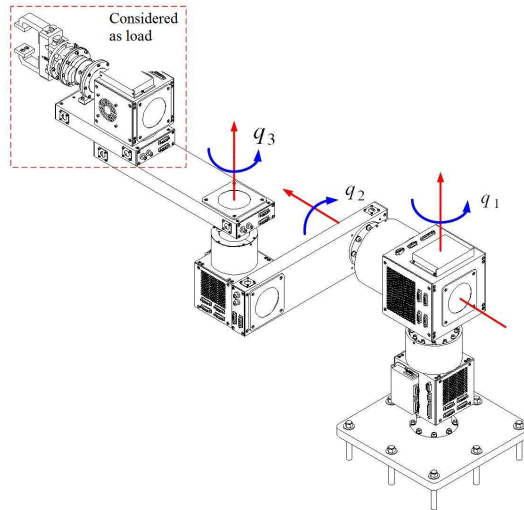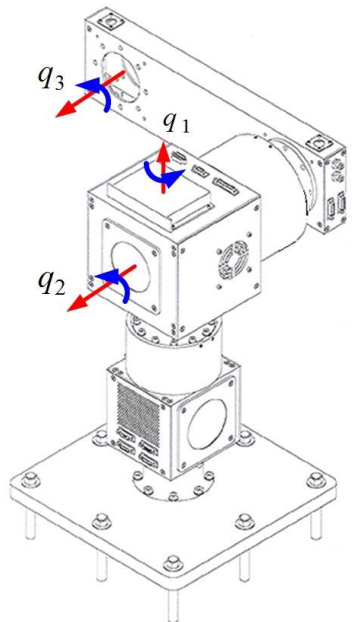

Figure 5.10: configuration 2: without load (The last joint is not shown)

in Fig.(5.23)-(5.34). In order to compare the performance of PID and proposed robust controller, the mean squared error results are summarized in tables 5.3 - 5.6. The mean squared error is calculated based ont the equation 5.4, and the percentage improvement of robust over PID controller is calculated using equation 5.5:

$$MSE_i = \frac{\sum_{j=1}^{N}(q_{d_{ij}} - q_{a_{ij}})^2}{N} \tag{5.4}$$

Where N is the number of sampled data, $i = 1, 2, 3$ refers i^{th} joint, and $q_{d_{ij}}$ and $q_{a_{ij}}$ are the desired and actual position of each joint, respectively.

$$improvement = \frac{PID(MSE) - robust(MSE)}{PID(MSE)} \times 100\% \tag{5.5}$$

From those tables, we can conclude that the proposed robust controller have a better performance in MRR position control. In addition, the joint 3 (Fig.(5.6)) has the larger mean squared error than that of joint 1 and 2. This is due to the fact that the dynamic interaction is increasing from the base to the end effector.

Figure 5.11: Joint 1 position error comparison in configuration 1 without load

Figure 5.12: Joint 1 torque comparison in configuration 1 without load

Figure 5.13: Joint 2 position error comparison in configuration 1 without load

Figure 5.14: Joint 2 torque comparison in configuration 1 without load

Figure 5.15: Joint 3 position error comparison in configuration 1 without load

Figure 5.16: Joint 3 torque comparison in configuration 1 without load

Figure 5.17: Joint 1 position error comparison in configuration 1 with load

Figure 5.18: Joint 1 torque comparison in configuration 1 with load

Figure 5.19: Joint 2 position error comparison in configuration 1 with load
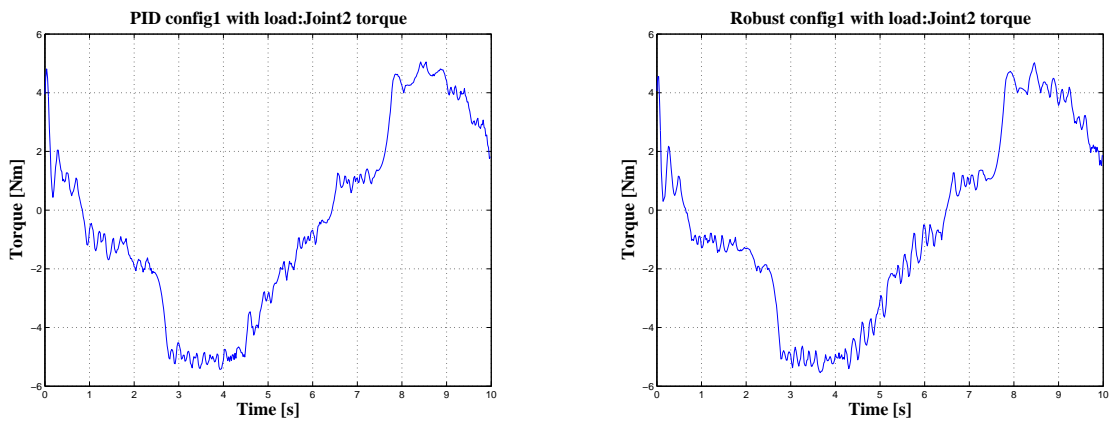
Figure 5.20: Joint 2 torque comparison in configuration 1 with load
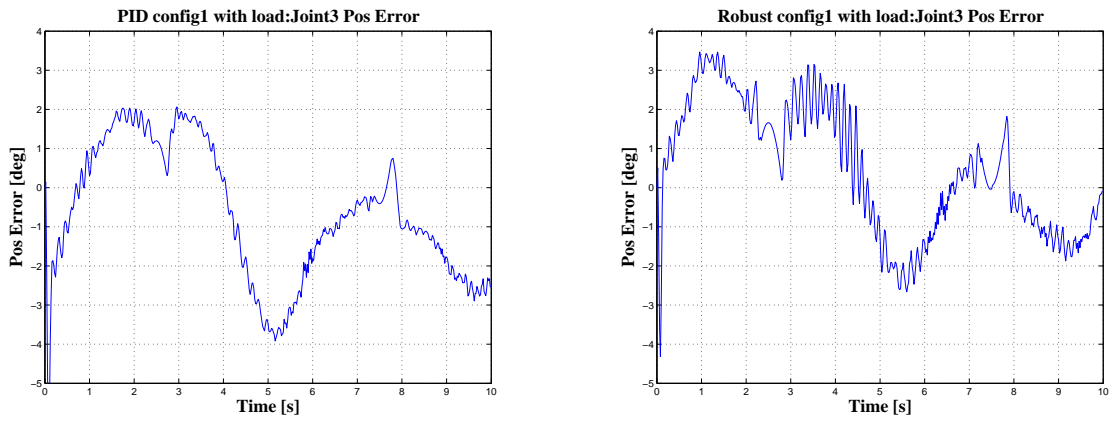
Figure 5.21: Joint 3 position error comparison in configuration 1 with load
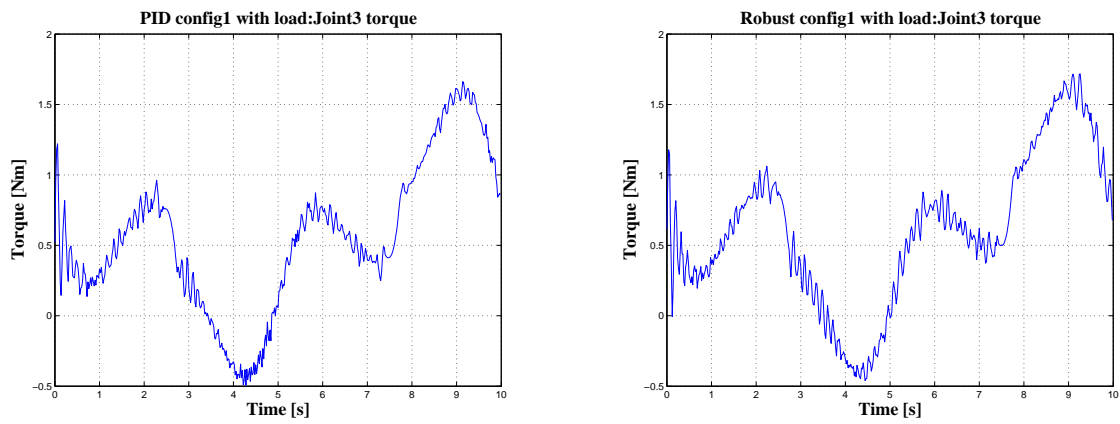
Figure 5.22: Joint 3 torque comparison in configuration 1 with load
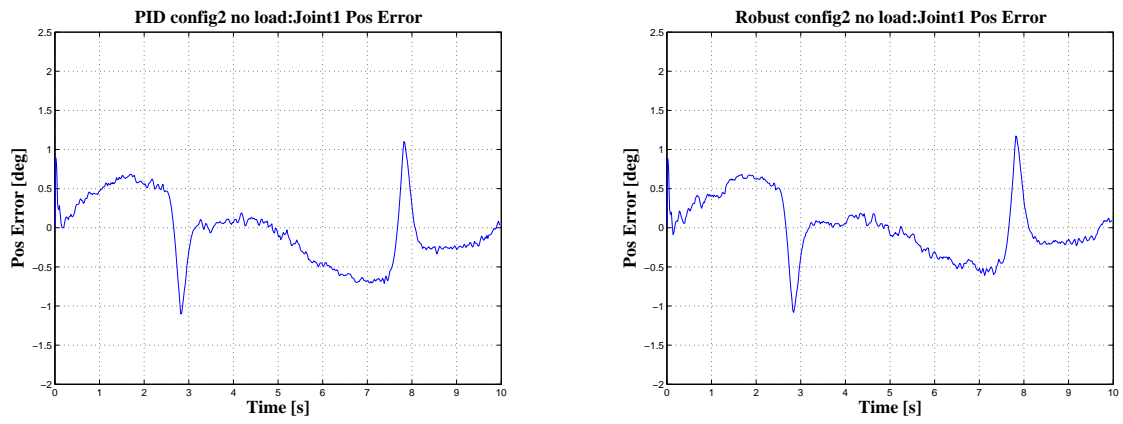
Figure 5.23: Joint 1 position error comparison in configuration 2 without load
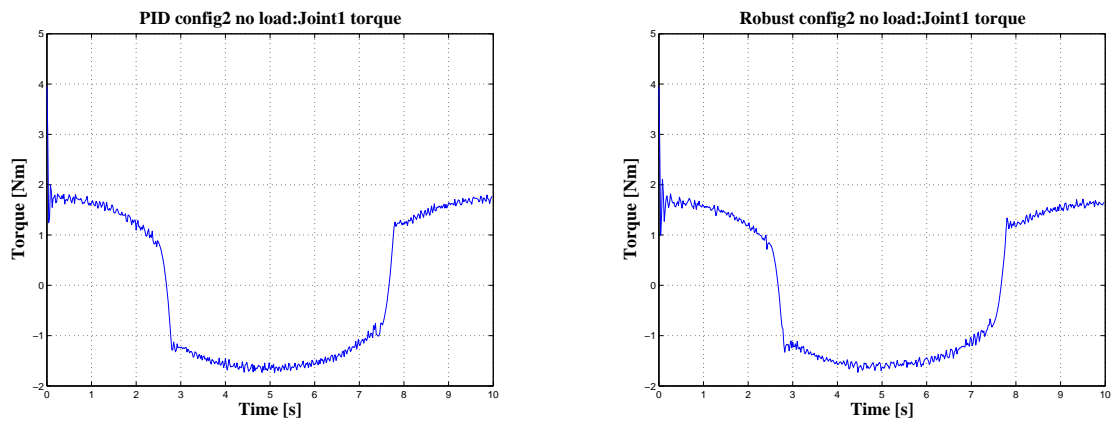
Figure 5.24: Joint 1 torque comparison in configuration 2 without load
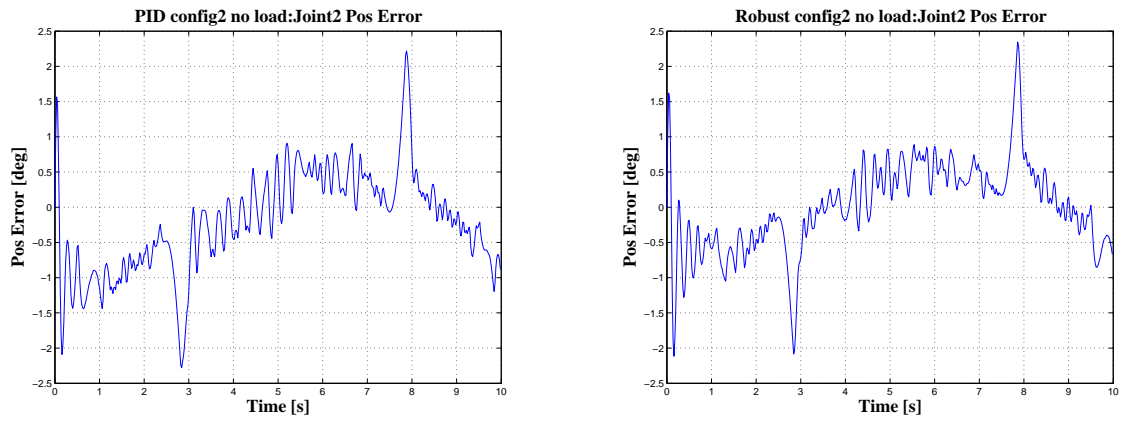
Figure 5.25: Joint 2 position error comparison in configuration 2 without load
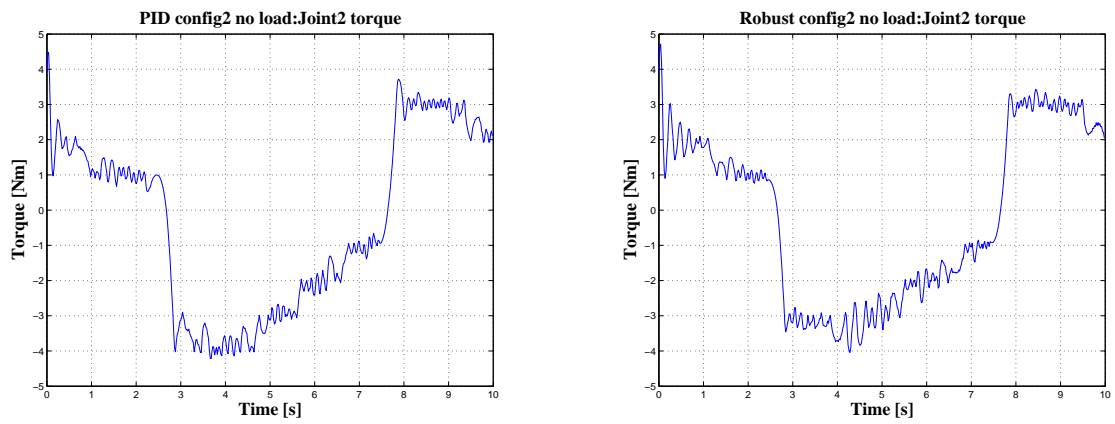
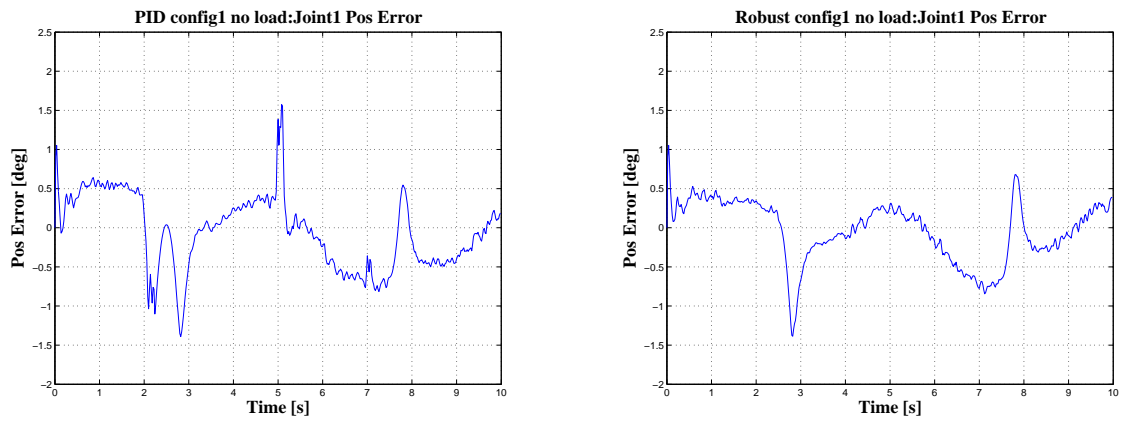Figure 5.26: Joint 2 torque comparison in configuration 2 without load
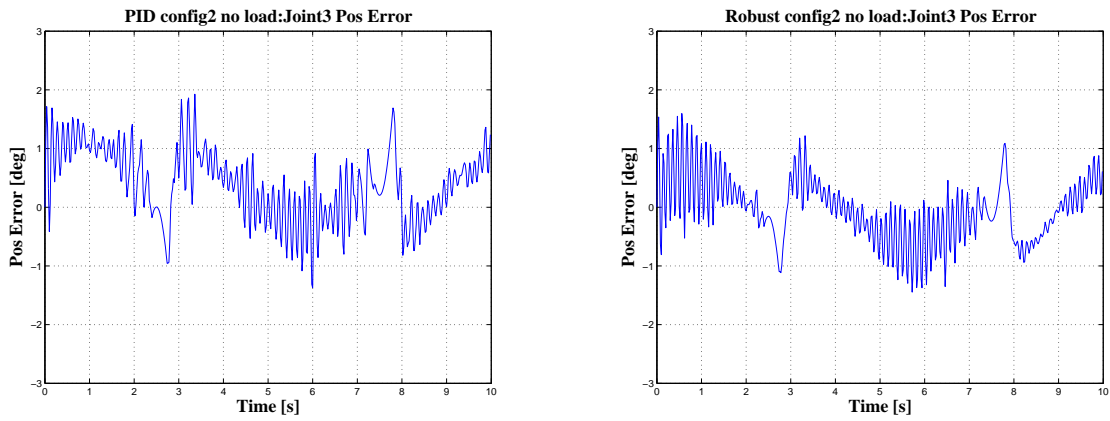
Figure 5.27: Joint 3 position error comparison in configuration 2 without load
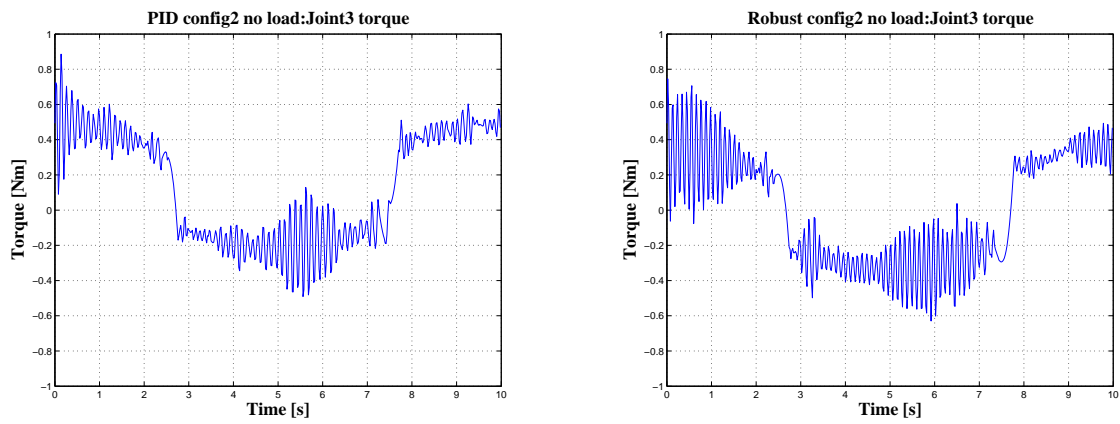
Figure 5.28: Joint 3 torque comparison in configuration 2 without load
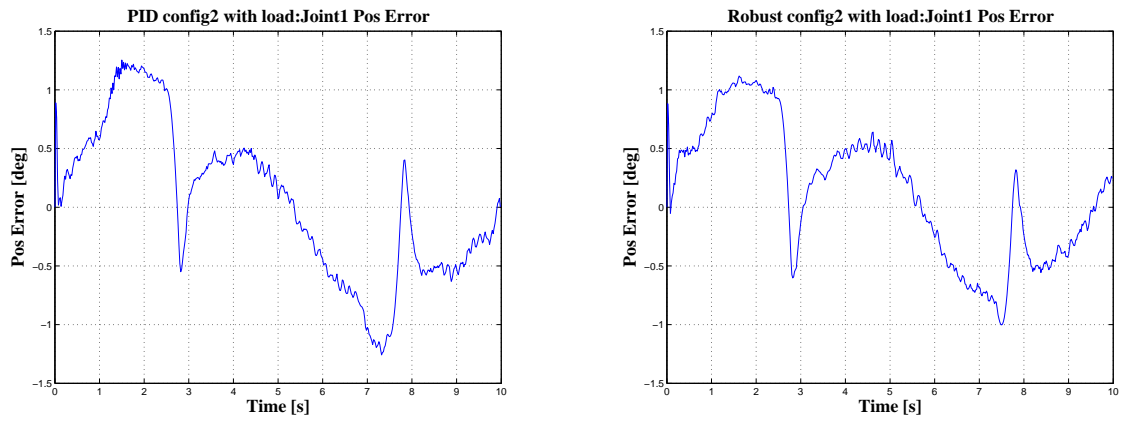
Figure 5.29: Joint 1 position error comparison in configuration 2 with load
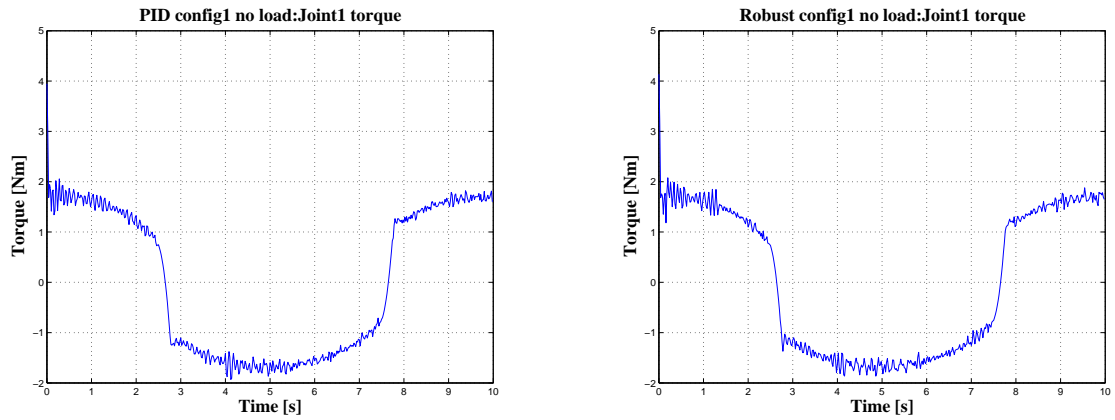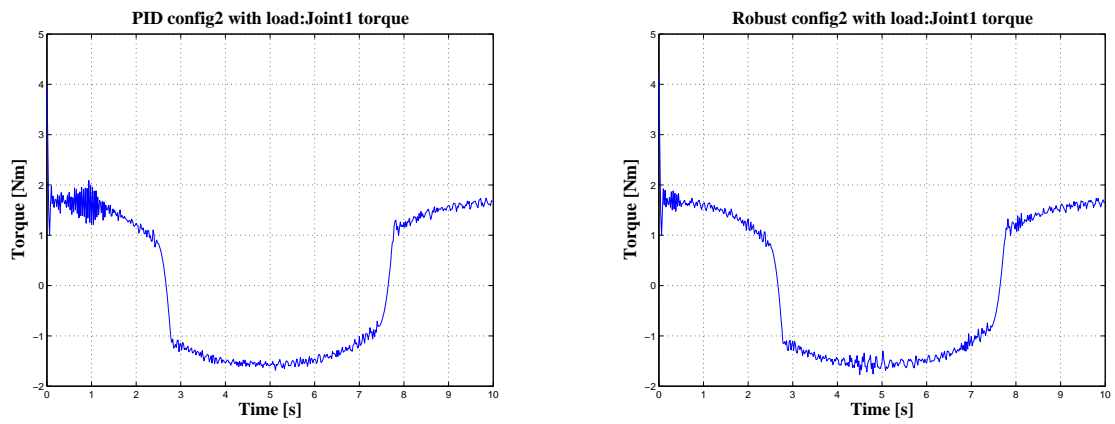

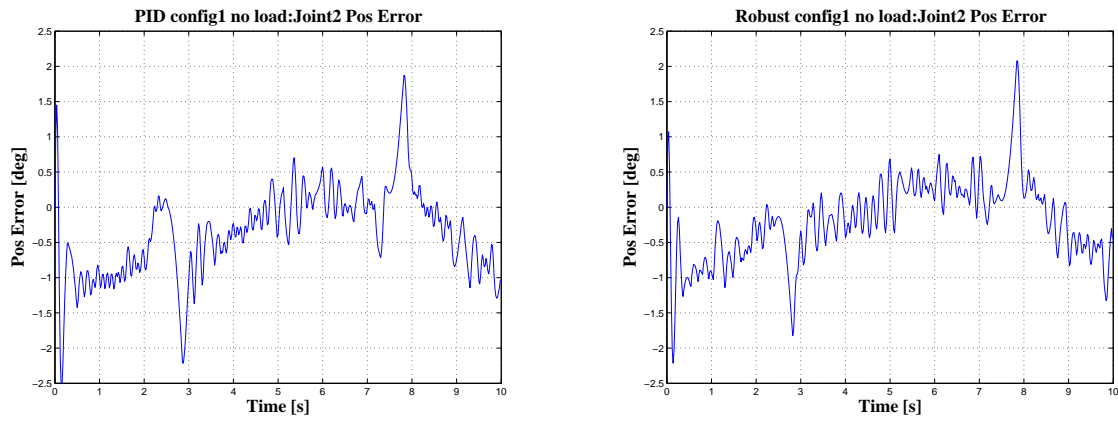Figure 5.30: Joint 1 torque comparison in configuration 2 with load
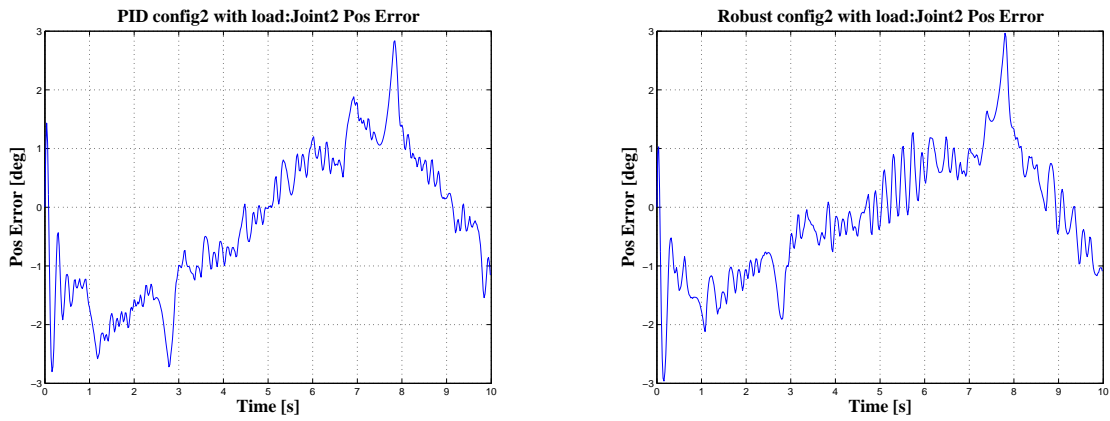
Figure 5.31: Joint 2 position error comparison in configuration 2 with load

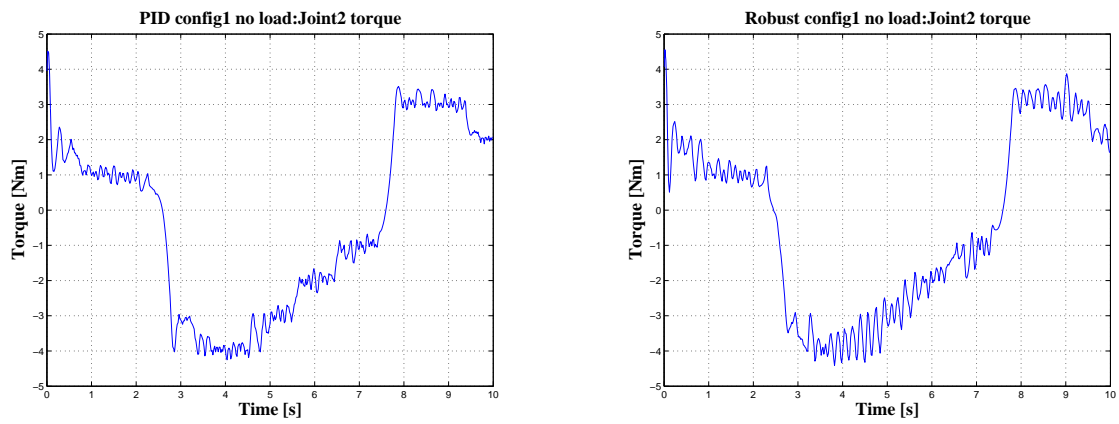
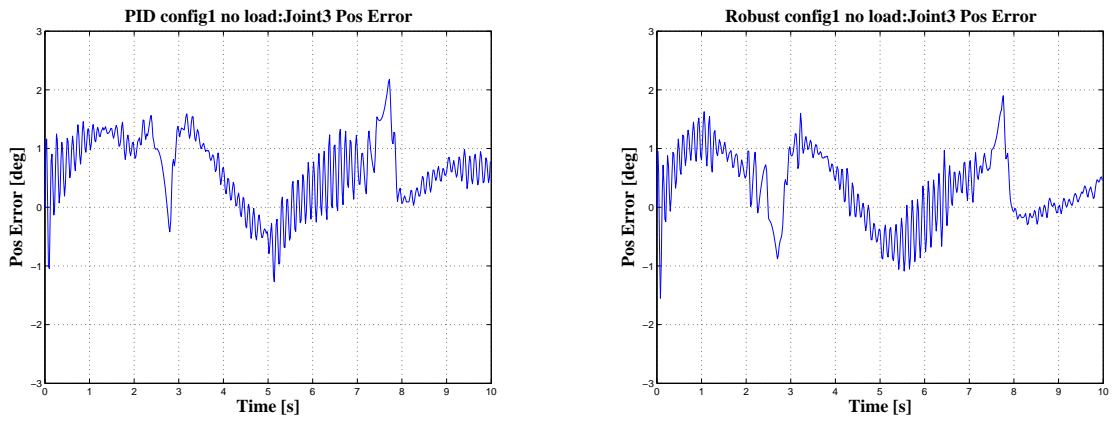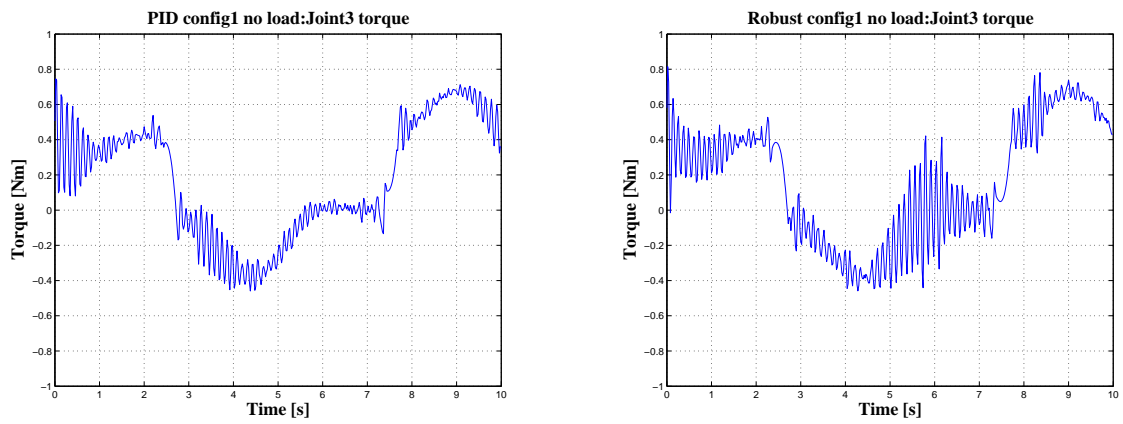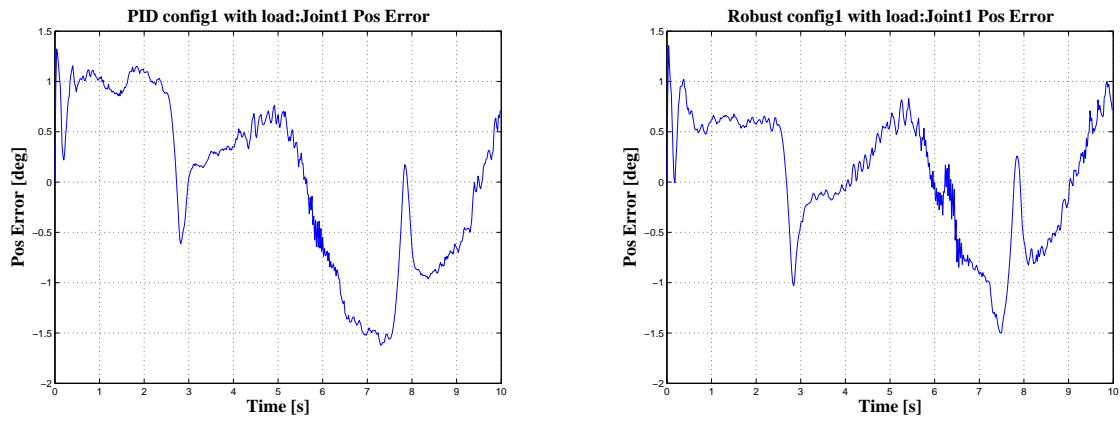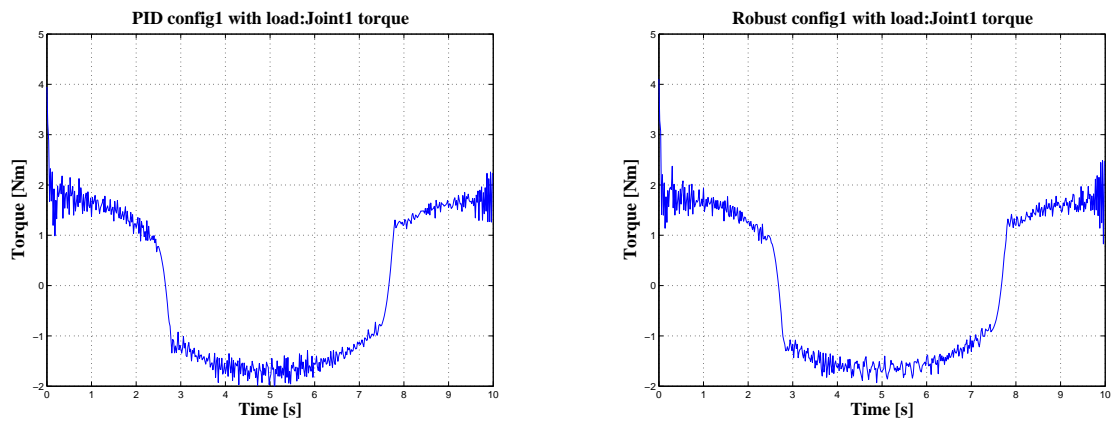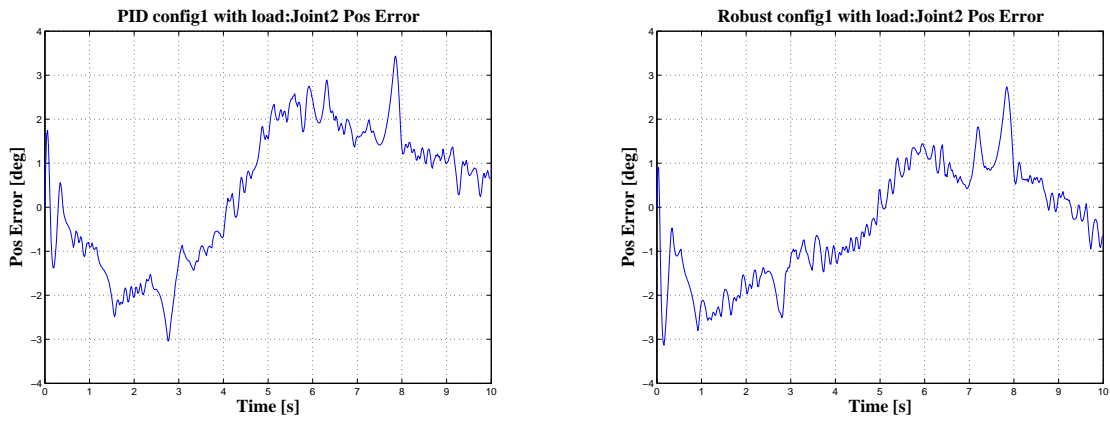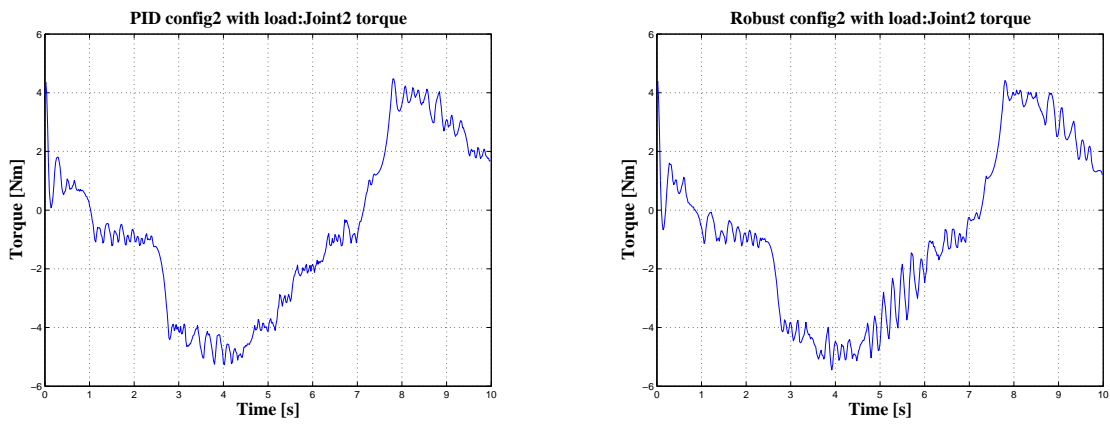Figure 5.32: Joint 2 torque comparison in configuration 2 with load
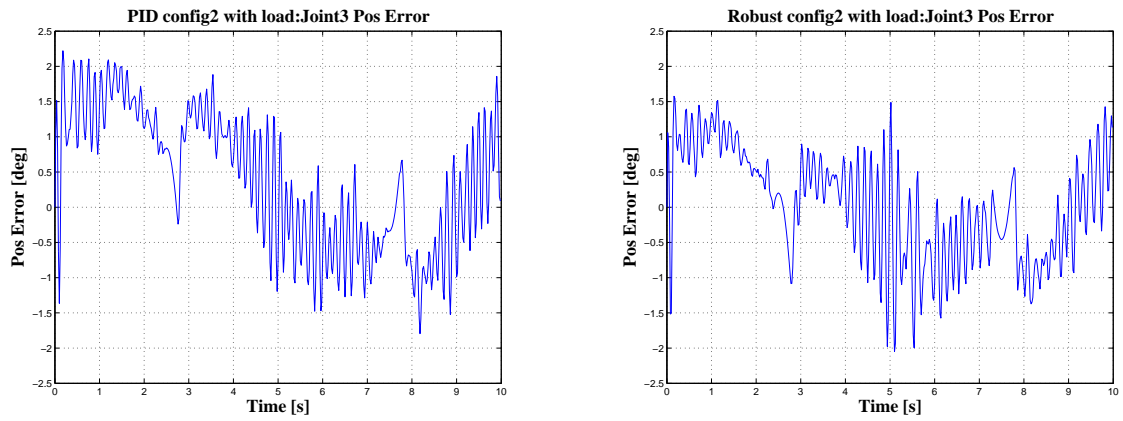
Figure 5.33: Joint 3 position error comparison in configuration 2 with load
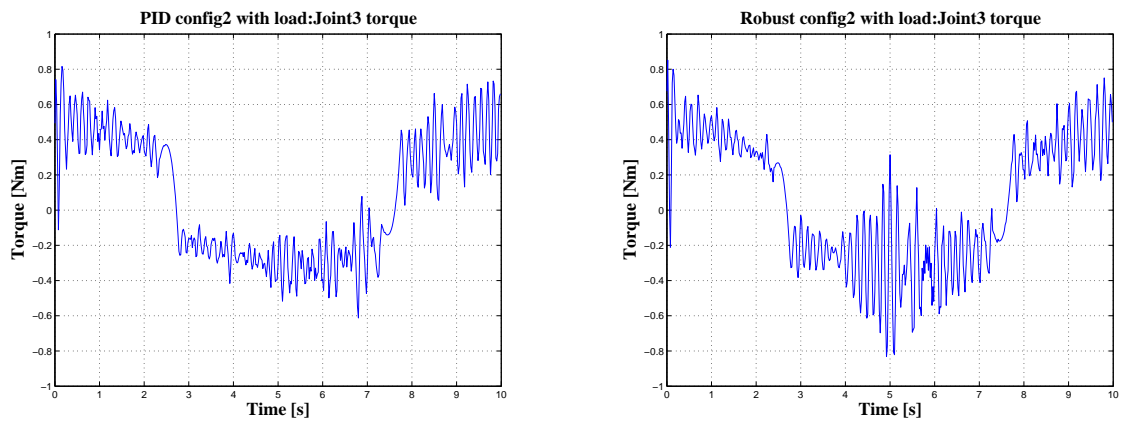
Figure 5.34: Joint 3 torque comparison in configuration 2 with load

5.3   Discussion

Parameters of the proposed controller were tuned to reduce the trajectory tracking error based on the first configuration without load, and satisfied the constraints described in chapter 4. We first tuned PD gain, K_3 and K_4 in equation (4.43), to achieve a good tracking

Table 5.3: comparison between PID and robust in configuration 1 without load

Degree of Freedom	PID (deg) Mean squared errors	Robust (deg) Mean squared errors	%Improvement of robust over PID
Joint 1	0.2290	0.1527	33.32
Joint 2	0.5191	0.3675	29.20
Joint 3	0.7540	0.4744	37.08

Table 5.4: comparison between PID and robust in configuration 1 with load

Degree of Freedom	PID (deg) Mean squared errors	Robust (deg) Mean squared errors	%Improvement of robust over PID
Joint 1	0.7023	0.3668	47.77
Joint 2	2.5363	1.7483	31.70
Joint 3	3.3558	3.0056	10.44

Table 5.5: comparison between PID and robust in configuration 2 without load

Degree of Freedom	PID (deg) Mean squared errors	Robust (deg) Mean squared errors	%Improvement of robust over PID
Joint 1	0.1797	0.1463	18.75
Joint 2	0.5623	0.4039	28.17
Joint 3	0.5234	0.3058	41.57

Table 5.6: comparison between PID and robust in configuration 2 with load

Degree of Freedom	PID (deg) Mean squared errors	Robust (deg) Mean squared errors	%Improvement of robust over PID
Joint 1	0.4160	0.3378	18.80
Joint 2	1.5943	1.0629	33.33
Joint 3	1.0777	0.586	45.62

performance. Then, the non-linear term was added to compensate for more disturbance and tuned to have a better performance.

To illustrate the proposed controller effectiveness in handling MRR reconfiguration, the same set of parameters were applied to all the other experiments, i.e. with load and the second configuration. Those parameters are listed in table 5.7. Please note that, parameters k_{ij}, $i = 1, 2$ and $j = 1, 2, 3, 4$, were not shown in this table, because they were calculated from equation (4.16) and (4.17), respectively.

Table 5.7: Robust Controller Parameters

Joint	linear parameters		nonlinear parameters			
	K_3	K_4	k_{30}	k_{31}	k_{32}	k_{33}
1	0.25	0.025	0.1	0.2	1	0.12
2	0.15	0.005	0.1	0.1	1	0.8
3	0.35	0.025	0.1	0.2	0.01	0.3

From Table 5.3, it can be shown that for configuration 1 the proposed robust controller outperformed the well-tuned linear controller for all three degrees of freedom. For the given trajectory in Fig.(5.8), the improvement in performance at no load is 33.32%, 29.20% and 37.08% for joint 1, 2, and 3, respectively. For a payload of 30Lb in the form of an end point wrist assembly, the improvement in performance using the robust controller is 47.77%, 31.7%, and 10.44% for joint 1, 2, and 3, respectively as shown in Table 5.4. Under

reconfigurability, all control parameters in Table 5.7 were kept unchanged. The robust control still outperformed the industrial linear control for the configuration 2 shown in Fig.(5.10). For the trajectory shown in Fig.(5.8) for all degrees of freedom, the robust control showed an improvement in tracking performance of 18.75% for joint 1, 28.17% for joint 2 and 41.57% for joint 3 at no load as shown in Table 5.5. With a 30Lb end point load, the improvement in tracking performance is 18.80% for joint 1, 33.33% for joint 2 and 45.62% for joint 3 as shown in Table 5.6.

From the experimental analysis results, we can see that the first joint, which is the base joint, has a better performance for all experiments. The third joint, which is the last one in the MRR joint/link chain, exhibits the worst performance with large oscillations in some cases. This observation indicates that the disturbance effect from the load side to the base side is more significant than that from the base side to the load side. In addition, the ESI MRR system has large joint/link inertia to joint output power ratio, so that there is more vibration at start, stop and direction transition point.

To assess the repeatability and accuracy of the robust control, we conducted 10 trails for each experimental scenarios (e.g. configuration 1/2, with/without load). The statistics analysis are listed in tables A.1-A.12 in appendix A.

Overall, the performance of the robust controller is satisfactory, given the fact that we applied the same controller parameters set in all experiments.

Chapter 6

Conclusion and Future Work

6.1 Conclusion

In this research, we developed, modeled, calibrated and controlled a modular and reconfigurable robot (MRR) for flexible automation.

Three joint modules have been manufactured. Each one has two input and two output connection ports, so that can be used as either a rotary joint or pivotal joint. The most advantage of this design is the zero offset when used as a pivotal joint. Also, the key/keyway sets ensure the reposition and reorientation accuracy. Cylinder type of links are designed to connect joints together. Using the developed joints and links, a vide variety of the MRR configurations can be constructed.

The derivation of single joint dynamics is also presented. In this model, each joint of the MRR system is considered as an independent unit. The dynamic effects from the other joints or links are treated as disturbance. In order to better understand the MRR system dynamic behaviors, a nonlinear harmonic drive (HD) model was applied and the HD flexspline stiffness and friction coefficients were calibrated experimentally.

By considering the MRR system properties,(dynamics changes with the change of configurations, uncertainties from complex HD gear meshing mechanisms, variation and unknown payload, etc), a decentralized robust control algorithm was developed using directlyapunov method and backstepping techniques.

The proposed controller was validated by computer simulation and experiments. In

the simulation, a velocity observer was used to predict the actual motor and joint velocity based on the approach in [52]. But for experiments, the actual velocity is provided by the motor drive through direct differentiation and filtering of the position signal. A sinusoidal trajectory for each joint was used for both simulation and experiments. In addition, we also conducted MRR position control using a PID controller, and compared the performance with that of the proposed robust controller. From the experimental results we concluded that: 1) the proposed robust controller has a better performance over PID controller, and 2) the large error for each joint occurs at the position where the joint changes its rotation direction, which causes significant disturbance due to link/load inertial dynamic effects.

6.2   Future Work

The first MRR prototype has been manufactured. For the current MRR design, some issues should be considered for the future system realization:

1. The size and weight of the medium and the largest joints are larger than expected. They can be reduced by using frameless motor while maintaining the rated power/torque requirements.

2. In order to achieve quick reconfiguration, some quick connection mechanism should be studied.

3. Running all cables and wires internally will be a challenging job. To deal with this, we need not only novel designed connectors, but also compact motor driver and controller which can be integrated inside the joint module.

4. The same experimental results performed on ESI MRR need t be repeated for the MRR proposed in this thesis to further validate the control performance.

5. Special design methodologies for the end tool should be implemented. By integrating a 4th and 5th degree of freedom together with a modular end tool, additional industrial tasks that require higher motion dexterity can be accomplished.

6. More research needs to be performed to identify means for "quicker" reconfigurability. Perhaps an easier way to connect joints to links is through the usage of specially designed latches as opposed to screws.

Appendix A

Experimental Results Statistic Analysis

In this appendix, the statics analysis of the experiments that evaluate the repeatability and accuracy of the robust control is presented. We calculated the mean, variance and standard deviation of each trial for each experimental scenario, i.e. different configurations, and with/without load.

Table A.1: Statistics results: Joint 1 configuration 1 without load

test #	mean	variance	standard deviation
1	-0.087	0.182	0.427
2	-0.079	0.157	0.396
3	-0.046	0.168	0.411
4	-0.051	0.060	0.401
5	-0.035	0.151	0.389
6	-0.043	0.150	0.388
7	-0.075	0.186	0.432
8	-0.074	0.189	0.435
9	-0.087	0.190	0.436
10	-0.089	0.192	0.438

Table A.2: Statistics results: Joint 2 configuration 1 without load

test #	mean	variance	standard deviation
1	-0.143	0.388	0.623
2	-0.317	0.305	0.553
3	-0.156	0.375	0.612
4	-0.149	0.347	0.589
5	-0.187	0.333	0.577
6	-0.181	0.355	0.595
7	-0.147	0.386	0.621
8	-0.153	0.395	0.629
9	-0.265	0.379	0.615
10	-0.113	0.422	0.649

Table A.3: Statistics results: Joint 3 configuration 1 without load

test #	mean	variance	standard deviation
1	0.359	0.299	0.547
2	0.609	0.365	0.604
3	0.297	0.545	0.54
4	0.303	0.328	0.573
5	0.334	0.363	0.602
6	0.340	0.330	0.574
7	0.339	0.295	0.543
8	0.350	0.322	0.567
9	-0.555	0.237	0.487
10	0.321	0.275	0.524

Table A.4: Statistics results: Joint 1 configuration 1 with load

test #	mean	variance	standard deviation
1	0.0678	0.4664	0.6829
2	0.0751	0.4553	0.6747
3	0.0603	0.3639	0.6032
4	-0.1645	0.8162	0.9034
5	-0.0328	0.6190	0.7868
6	-0.0321	0.6137	0.7834
7	0.1034	0.4248	0.6518
8	0.1322	0.3953	0.6287
9	0.1637	0.4059	0.6371
10	0.1879	0.3712	0.6093

Table A.5: Statistics results: Joint 2 configuration 1 with load

test #	mean	variance	standard deviation
1	0.8145	1.9572	1.3990
2	0.8609	2.0358	1.4268
3	-0.3823	1.6054	1.2670
4	0.3582	1.5899	1.2609
5	0.1179	1.8016	1.3422
6	0.4279	1.8624	1.3647
7	0.8630	2.0251	1.4231
8	0.8588	2.0436	1.4295
9	0.8536	2.1223	1.4568
10	0.8616	2.1399	1.4628

Table A.6: Statistics results: Joint 3 configuration 1 with load

test #	mean	variance	standard deviation
1	-1.4633	2.9670	1.7225
2	-1.5487	3.0153	1.7365
3	0.4585	2.8010	1.6736
4	-0.3338	1.6561	1.2869
5	-0.1872	2.7184	1.6488
6	-0.6806	2.6251	1.6202
7	-1.5980	2.9975	1.7313
8	-1.6353	3.0816	1.7555
9	-1.6772	3.1032	1.7616
10	-1.7275	3.0915	1.7583

Table A.7: Statistics results: Joint 1 configuration 2 without load

test #	mean	variance	standard deviation
1	0.0499	0.1449	0.3807
2	0.0104	0.4046	0.6361
3	0.0113	0.4032	0.6350
4	-0.2457	1.1865	1.0893
5	-0.0731	0.5263	0.7254
6	0.0408	0.4581	0.6769
7	0.0117	0.4574	0.6763
8	0.0217	0.4740	0.6637
9	0.0317	0.4462	0.7563
10	-0.0524	0.3987	0.6314

Table A.8: Statistics results: Joint 2 configuration 2 without load

test #	mean	variance	standard deviation
1	-0.0301	0.3562	0.5968
2	-0.0376	0.3050	0.5523
3	-0.0493	0.3186	0.5644
4	0.2628	0.8562	0.9253
5	0.1407	0.4077	0.6386
6	0.0875	0.2890	0.5376
7	0.2105	0.2414	0.4913
8	0.1100	0.3141	0.5931
9	0.156	0.3414	0.4133
10	0.2324	0.2515	0.5015

Table A.9: Statistics results: Joint 3 configuration 2 without load

test #	mean	variance	standard deviation
1	-0.0238	0.2601	0.5100
2	0.0162	0.1463	0.3825
3	0.0203	0.1454	0.3814
4	0.0884	0.4317	0.6571
5	-0.0063	0.2284	0.4779
6	-0.0856	0.1571	0.3963
7	-0.0882	0.1442	0.3797
8	-0.0721	0.1221	0.3598
9	-0.0782	0.1561	0.3289
10	-0.0875	0.1437	0.3790

Table A.10: Statistics results: Joint 1 configuration 2 with load

test #	mean	variance	standard deviation
1	0.1919	1.0832	1.0408
2	0.1232	1.0650	1.0320
3	0.0748	1.0817	1.0400
4	0.0781	1.0937	1.0456
5	-0.0241	1.0668	1.0329
6	-0.0212	1.0687	1.0291
7	-0.1624	1.0386	1.0191
8	0.1840	1.1224	1.0594
9	0.1459	1.1687	1.0810
10	0.0681	1.1401	1.0678

Table A.11: Statistics results: Joint 2 configuration 2 with load

test #	mean	variance	standard deviation
1	-0.5578	0.5327	0.7298
2	-0.4608	0.5510	0.7423
3	-0.4332	0.5547	0.7673
4	-0.4220	0.5427	0.7367
5	-0.2412	0.5489	0.7409
6	-0.2300	0.5891	0.7002
7	0.0200	0.5867	0.7660
8	-0.5176	0.7618	0.8728
9	-0.5011	0.7916	0.8926
10	-0.2834	0.6267	0.7916

Table A.12: Statistics results: Joint 3 configuration 2 with load

test #	mean	variance	standard deviation
1	0.1480	0.3474	0.5894
2	0.1557	0.3596	0.5997
3	0.1811	0.3102	0.5955
4	0.1803	0.3527	0.5939
5	0.1589	0.3566	0.5971
6	0.1425	0.3495	0.5001
7	0.1377	0.3195	0.5652
8	0.1336	0.3489	0.5907
9	0.1421	0.3569	0.5974
10	0.1021	0.3648	0.6040

Bibliography

[1] I. -M. Chen and G. Yang,Configuration independent kinematics for modular robots. *IEEE Int. Conf. Robotics and Automation*,Minneapolis, MN, pp. 1440-1445, 1996.

[2] D. Schmitz, P. Khosla and T. Kanade, The CMU reconfigurable modular manipulator system. Carnegie Mellon Univ., CMU-RI-TR-88-7, 1988.

[3] T. Matsumaru, Design and control of the modular robot system: TOMMS, *IEEE International Conference on Robotics and Automation*, 0-7803-1965-6, pp. 2125 - 2131, 1995

[4] Z.M.Bi and S.Y.T.Lang, General modular robot architecture and configruation design, *Proceeding of the IEEE International Conference on Mechatronics and Automation*, Niagara Falls, Canada, pp. 268 - 273, July 2005

[5] G.Yang, I-M.Chen, W.K.Lim, and S.H.Yeo, Design and kinematic analysis of modular reconfiguralbe parallel robots, *Proceddings of IEEE International Conference on Robotics and Automation*, Detroit, Michigan, pp. 2501 - 2506, May 1999

[6] J-K. Choi, T. Omata, and O. Mori, Self-reconfiguralbe planar parallel robot, *Proceeding of 2004 IEEE/RSJ International Conference on Intelligent Robots and Systems*, Sendai, Japan, pp, 2654 - 2660, 2004

[7] D.Zhang and Z. Bi, Development of reconfigurable parallel kinematic machines using modular design approach, *CDEN/RCCI International Design Conference*, University of Torronto, Ontario, Canada, July 2006

[8] G.Yang, I-Ming Chen, W.Chen and S.H.Yeo, Design and analysis of a 3-RPRS modular parallel manipulator for rapid deployment, *Proceedings of IEEE/ASME International Conference on Advanced Intelligent Mechatronics*, pp. 1250 - 1255, 2003

[9] J.Zhao, Z.Ren and Y.Zhang, Configuration matching in self-reconfigurable process of modular self-reconfiguralbe robots. *Proceedings of IEEE International Conference on Mechatronics and Automation*, Luoyang, China, pp. 284 - 288, June 2006

[10] D.G.Duff, M.Yim and K.Roufas, Evolution of PolyBot: A modular reconfigurable robot.

[11] A.Brunete, M.Hernando and E.Gambao, Modular multiconfiguralbe architecture for low diameter pipe inspection microrobots, *Proceedings of IEEE International Conference on Rrobotics and Automation*, Barcelona, Spain, pp. 490 - 495, April 2005

[12] S.Murata and H. Kurokawa, Self-reconfiguralbe robots, Department of Computational Intelligence and Systems Science, Tokyo Institute of Technology, Nagatsuda, Midori, Yokohama, Japan

[13] P.Jantapremjit and D.Austin, Design of a modular self-reconfigurable robot, *Proceeding Austrilian Conference on Robotics and Automation*, Sydney, pp. 38 - 43, November 2001

[14] D.M.Hensinger, G.A.Johnston, E.M.Hinman-Sweeney, J.Feddema and S.Eskridge, Self-reconfigurable robots, Sandia National Laboratories, Octoober 2002

[15] I.-M. Chen, Theory and applications of modular reconfigurable robotic system. Ph. D thesis, California Institute of Technology, CA, 1994.

[16] N. A. Aspragathos, Reconfigurable robots towards the manufacturing of the future. *Virtual conference in Reconfigurable Manufacturing Systems*, IPROM, 2005

[17] J. Han, W. K. Chung, Y. Youm and S.H. Kim, Task based design of modular robot manipulator using efficient genetic algorithm. *Proceedings of IEEE International Conference on Robotics and Automation*, Albuquerque, New Mexico,p507-512, April 1997

[18] H.Asada and J.J.E.Slotine, Robot analysis and control, John Wiley and Sons, N.Y, 1986

[19] C.J.J.Paredis, H. B. Brown, P. K. Khosla, A rapidly deployable manipulator system. *Prodeedings of IEEE International Conference on Robotics and Automation*, Minneapolis, Minnesota, p1434-1439, April 1996

[20] D.B.Stewart, and P.K.Khosla, Rapid development of robotics applications using component-based real-time software. *Proceddings of the IEEE/RSJ International Conference on Intelligent Robots and Systems*, Pittsburgh, Pennsylvania, August, vol. 1. pp 465-470, 1995

[21] I.-M Chen, Rapid response manufacturing through a rapidly reconfiguralbe robotic workcell. *Robotics and Computer Integrated Manufacturing*. p199-213, 17(2001)

[22] S.Shi, X. Gao, Z, Xie, F. Ni, H. Liu, E. Kraemer and G. Hirzinger, Development of reconfigurable space robot arm. *1st International Symposium on Systems and Control in Aerospace and Astronautics*, p138-143, 2006

[23] G. Hirzinger, A. Albu-Schaffer, M. Hahnle, I. Schaefer, N. Sporer, On a new generation of torque controlled light-weight robots. *Proceedings of IEEE int. Conf. on Robotics and Automation*, Seoul, Korea, 3356-3363, 2001

[24] T. Matsumaru, Design and control of the modular robot system: TOMMS. *Proceedings of the IEEE International Conference on Robotics and Automation*, Nagoya, Japan, p2125-2131, 1995

[25] K. H. Hunt, Kinematic geiometry of mechanisms. New York, NY, Oxford University Press, 1978

[26] A. D. Luca, R. Farina, P. Lucibello, On the control of robots with visco-elastic joints. *Proceeding of IEEE International Conference on Robotics and Automation*, Barcelona, Spain, 2005.

[27] N. Kircanski and A.A.Goldenberg, An experimental study of nonlinear stiffness, hysteresis, and friction effects in robot joints with harmonic drives and torque sensors. *International Journal of Robotics Research*, Vol. 16. No. 2, pp.214-239, April 1997

[28] T.D.Tuttle and W. Seering, Modeling a harmonic drive gear transmission. *IEEE International Conference on Robotics and Automation*, vol.2, pp.624-629, May 1993

[29] R.Dhaouadi, F.H.Ghorbel and P.S.Gandhi, A new dynamic model of hysteresis in harmonic drives. *IEEE Transactions on Industrial Electronics*, vol. 50, No.6, pp. 1165-1171, December 2003

[30] H.D.Taghirad and P.R.Belanger, A nonlinear model for harmonic drive friction and compliance. *IEEE International Conference on Robotics and Automation*, pp.1-6, 1998

[31] H. Seraji, Adaptive independent joint control of manipulators: theory and experiment. *Proceeding of IEEE international conference on Robotics and Automation*, p854-61 vol.2, 1998

[32] Y. Tang, M. Tomizuka, G. Guerrero, and G. Montemayor, Decentralized robust control of mechanical systems. *IEEE Transaction on Automationand Control*,vol. 26, pp. 1139-1144, 1981

[33] M. Erlic and W. S. Lu, A reduced-order adaptive velocity observer for manipulator control. *IEEE Trans. Robotics and Automation*, vol 11, NO. 2, 1995.

[34] T. C. S. Hsia, A. Lasky, and Zhengyu Guo, Robust independent joint controller design for industrial robot manipulators. *IEEE Trans. on Industrial Electronics*, vol. 38, NO. 1, 1991.

[35] A. Rodrguez. Angeles and H. Nijmeijer, Synchronizing tracking control for flexible joint robots via estimated state feedback. *Transactions of the ASME*, vol. 126, pp. 162-172, 2004.

[36] H. D. Taghirad and M. A. Khosravi, Stability analysis and robust composite controller synthesis for flexible joint robots. *Advanced Robotics*, vol. 20, NO. 2, pp. 181-211, 2006.

[37] D. M. Dawson, Z. Qu, M. Bridges, and J. Carroll, Robust tracking of rigid-link flexible-joint electrically-driven robots. *Proceedings of IEEE conference on Decision and Control*, Brighton, England, pp. 1409-1412, 1991.

[38] V. Etxebarria, A. Sanz and I. Lizarraga, control of a lightweight flexible robotic arm using sliding modes. *International Journal of Advanced robotic Systems*, vol. 2, pp. 103-110, 2005.

[39] M. W. Spong, Modeling and control of elastic joint robots. *Journal of Dynamic Systems, Measurements, and Control*, vol. 109, pp. 310-319, 1987.

[40] H. D. Taghirad and M. A. Khosravi, Stability analysis and robust composite controller synthesis for flexible joint robots. *Advanced Robotics*, vol. 20, NO. 2, pp. 181-211, 2006.

[41] H. D. Taghirad and S. Ozgoli, Robust controller with a supervisor implemented on a flexible joint robot. *Proceeding of IEEE Conference on Control Applications*, pp. 1188-1193, 2005.

[42] H. G. Sage, M. F. DE Mathelin and E. Ostertag, Robust control of robot manipulators: a survey. *International Journal of Control*,72(16), 1498-1522, 1999.

[43] Z. Qu and D. M. Dawson, Robust tracking control of robot manipulators. The Institute of Electrical and Electronics Engineers, Inc., NJ, pp.120-126, 1996.

[44] F. L. Lewis, C. T. Abdallah and D. M. Dawson, Control of robot manipulators. Macmillan, NY, pp,189-255, 1993.

[45] Y. Tang, M. Tomizuka, G. Guerrero, and G. Montemayor, Decentralized robust control of mechanical systems. *IEEE Transactions on Automatic control*, vol. 45, NO. 4, pp. 771-776, 2000.

[46] M. Tarokh, Decoupled nonlinear three-term controllers for robot trajectory tracking. *IEEE Transactions on Robotics and Automation*, vol. 15, NO. 2, pp. 369-380, 1999.

[47] M. W. Spong, Seth Hutchinson and M. Vidyasagar, Robot modeling and control. John Wiley and Sons, Inc., NJ, pp. 348-357, 2006.

[48] M. M. Bridges and D. M. Dawson, Redesign of robust controllers for rigid-link flexible-joint robotic manipulators actuated with harmonic drive gearing. *IEE Proc. Control theory Appl.*, 142(5), 508-514, 1995.

[49] A. D Luca, B. Siciliano and L. Zollo, PD control with on-line gravity compensation for robots with elastic joints: Theory and experiments. *Automatica*, 41, 1809-1819, 2005.

[50] C. J. B. Macnab, G. M. T. D'Eleuterio and M. Meng, CMAC adaptive control of flexible-joint robots using backstepping with tuning functions. *IEEE Proc. International Conference on Robotics and Automation*, 2679-2686, 2004.

[51] C. J. B. Macnab, Z. Qu and R. Johnson, Robust fuzzy control for robot manipulators. *IEE Proc.Control Theory Appl.*, 147(2), 212-216, 2000.

[52] S. Y. Lim, D. M. Dawson, J. Hu and M. S. de Queiroz, An adaptive link position tracking controller for rigid-link flexible-joint robots without velocity measurements. *IEEE Transactions on Systems, MAN, and Cybernetics - part B: Cybernetics*, 27(3), pp. 412-427, 1997.

[53] T. D. tuttle and W. P. Seering, A nonlinear model of a harmonic drive gear transmission. *IEEE Transaction on Robotics and Automation*, 12(3), pp. 368-374, 1996.

[54] P.C. Chandrasekharan, robust control of linear dynamical systems, Academic Press, 1996.

[55] K.J. Astrom, Adaptive control around 1960, *IEEE control Systems*, 16(3), 1996, pp. 44-49

[56] D. Abramovitch, Some crisp thoughts on fuzzy logic, *Proceedings of the American Control Conference*, pp. 168-172, June 1994

[57] Z. Qu, Robust control of nonlinear uncertain systems, John wiley and Sons, 1998

[58] H.K. Khalil, Nonlinear systems,Prentice-Hall, Inc., NJ, pp589-603, 2002